NATIONAL ENERGY TECHNOLOGY LABORATORY

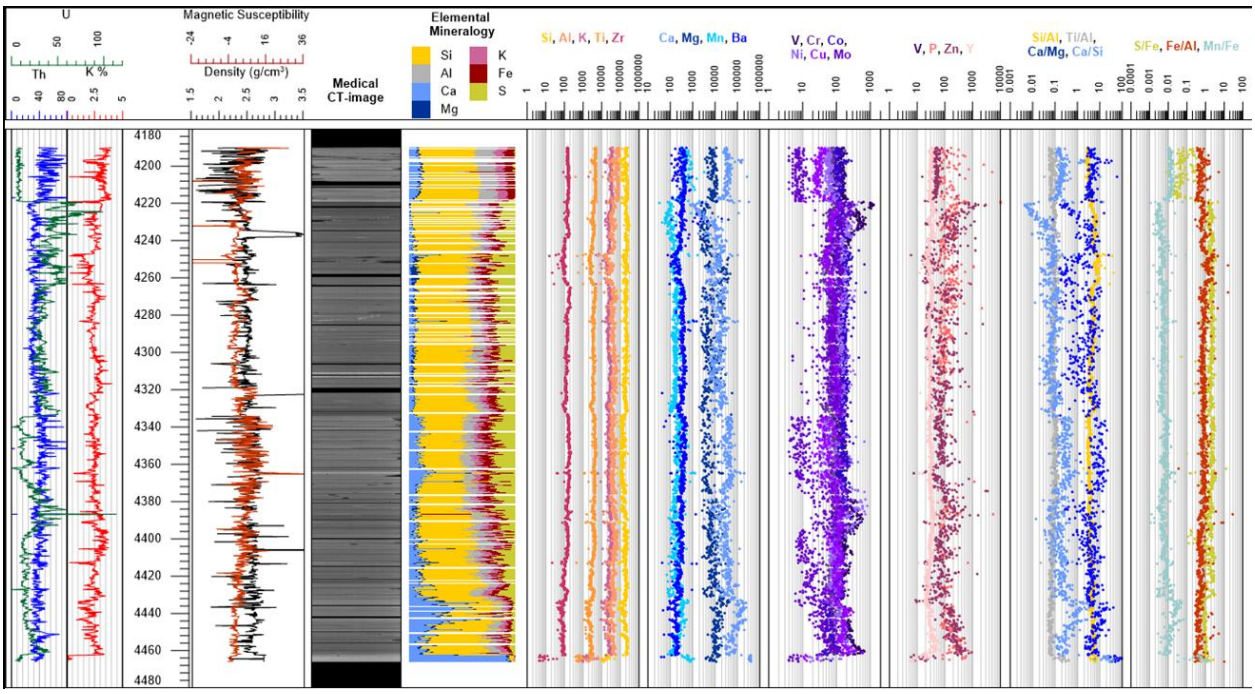

Computed Tomography Scanning and Geophysical Measurements of UW Enterprises LP 1-250512-129 Well in Southwestern Indiana

28 June 2024

U.S. DEPARTMENT OF ENERGY | NATIONAL ENERGY TECHNOLOGY LABORATORY

Office of Fossil Energy and Carbon Management

DOE.NETL-2024.4803

Disclaimer

This project was funded by the United States Department of Energy, National Energy Technology Laboratory, in part, through a site support contract.

Cover Illustration: Cropped compiled core log for the UW Enterprises LP 1-250512-129 Well; tracks 1 to 11 (uranium (green), thorium (blue), and potassium (red); depth (ft); density (red) and magnetic susceptibility (black); medical computed tomography images; X-ray fluorescence mineralogy; detrital elemental proxies; skeletal elemental proxies; redox elemental proxies, biogenic production proxies, and important elemental ratios); see Figure 31 for a detailed description.

Suggested Citation: Hu, L.; Paronish, T.; Crandall, D.; Jarvis, K.; Mitchell, N.; Brown, S.; Workman, S.; Douds, A.; Mastalerz, M., *Computed Tomography Scanning and Geophysical Measurements of the UW Enterprises LP 1-250512-129 Well in Southwestern Indiana;* DOE.NETL-2024.4803; NETL Technical Report Series; U.S. Department of Energy, National Energy Technology Laboratory: Morgantown, WV, 2024; p 48. DOI: https://doi.org/10.2172/2371703

An electronic version of this report can be found at:

https://netl.doe.gov/energy-analysis/search

The data in this report can be accessed from NETL's Energy Data eXchange (EDX) online system (https://edx.netl.doe.gov) using the following link:

https://edx.netl.doe.gov/dataset/uw-enterprises

Computed Tomography Scanning and Geophysical Measurements of the UW Enterprises LP 1-250512-129 Well in Southwestern Indiana

Lianbo Hu[1,2]; Thomas Paronish[1,2]; Dustin Crandall[1]; Karl Jarvis[1,2]; Natalie Mitchell[1,2]; Sarah Brown[1,2]; Scott Workman[1,2]; Ashley Douds[3]; Maria Mastalerz[3]

[1]National Energy Technology Laboratory, 3610 Collins Ferry Road, Morgantown, WV 26505, USA

[2]NETL Support Contractor, 3610 Collins Ferry Road, Morgantown, WV 26505, USA

[3]Indiana Geological & Water Survey, Indiana University, 1001 E 10th Street, Bloomington, IN 47405

DOE/NETL-2024/4803

28 June 2024

NETL Contacts:

Dustin Crandall, Principal Investigator

R. Burt Thomas, Technical Portfolio Lead

Bryan Morreale, Associate Laboratory Director for Research & Innovation, Research & Innovation Center

This page intentionally left blank.

Table of Contents

This page intentionally left blank.

List of Figures

List of Figures (cont.)

List of Tables

Acronyms, Abbreviations, and Symbols

Term	Description
2D	Two-dimensional
CM/REE	Critical mineral and rare earth elements
CT	Computed tomography
CTN	CT number
d	Sample thickness
DOE	U.S. Department of Energy
EDX	NETL's Energy Data eXchange
H	External magnetic field
HU	Hounsfield Units
I	Measured intensity
I_0	Source intensity
J	Magnetic response (per unit volume)
k	Volume susceptibility
MSCL	Multi-Sensor Core Logger
NETL	National Energy Technology Laboratory
v	Acoustic velocity
XRF	X-ray fluorescence
Z	Acoustic impedance
μ	Compton attenuation coefficient
ρ, ρ_B	Bulk density

Acknowledgments

This work was completed at the National Energy Technology Laboratory (NETL) with support from the U.S. Department of Energy's (DOE) Office of Fossil Energy Resource Sustainability Program. The authors wish to acknowledge Bryan Morreale (NETL Research & Innovation Center), Jessica Mullen (NETL Technology Development and Integration Center), and Mary Anne Alvin (DOE Office of Fossil Energy) for programmatic guidance, direction, and support.

The authors would like to thank Bryan Tennant for computed tomography data collection and technical support. Thank you to the staff of the Geologic Characterization, Analytics, and Modeling laboratory at NETL for continued laboratory support. The core was donated to the Indiana Geological and Water Survey by the Woolsey Operating Company.

ABSTRACT

The computed tomography (CT) facilities and the Multi-Sensor Core Logger (MSCL) at the National Energy Technology Laboratory (NETL) in Morgantown, West Virginia, were used to characterize Illinois Basin core of the Upper Devonian-Early Mississippian New Albany Shale Formation from Posey County, Indiana. The primary impetus of this work is a collaboration between Indiana Geological and Water Survey at Indiana University Bloomington, NETL, and Woolsey Operating Company LLC to characterize and make publicly available core information from the New Albany Shale of the Illinois Basin. Core characterization of this unconventional oil/gas well will aid in understanding the lithology changes and the fracture complexity of the New Albany Shale. There is a potential for this formation to be developed in the future for critical mineral and rare earth element (CM/REE) extraction. The resultant datasets are presented in this report and can be accessed from NETL's Energy Data eXchange (EDX) online system using the following link: https://edx.netl.doe.gov/dataset/uw-enterprises.

All equipment and techniques used were non-destructive, enabling future examinations and analyses to be performed on this core. None of the equipment used was suitable for direct visualization of the pore space in the fine-grained structures studied; however, fractures, discontinuities, and millimeter-scale features were readily detectable with the methods tested. Imaging with the NETL medical CT scanner was performed on the entire core. Targeted higher resolution CT scanning of select sections was performed with NETL's industrial and micro-CT scanner. Qualitative analysis of the medical CT images, coupled with X-ray fluorescence (XRF), P-wave, and magnetic susceptibility measurements from the MSCL were useful in identifying zones of interest for more detailed analysis. The ability to quickly identify key areas for more detailed study with higher resolution will save time and resources in future studies. The combination of methods used provides a multi-scale analysis of the core; the resulting macro and micro descriptions are relevant to many subsurface energy related examinations traditionally performed at NETL.

1. INTRODUCTION

Evaluation of core data from ongoing and emerging unconventional reservoirs have long been a priority of the U.S. Department of Energy's (DOE) National Energy Technology Laboratory (NETL). DOE has determined that the exploration and extraction of critical minerals and rare earth elements (CM/REE) in unconventional plays could help to establish energy independence and secure a larger domestic reserve of CMs/REEs. The goal of this report is to characterize and disseminate data from the UW Enterprises LP 1-250512-129 well (API#: 13-129-55088; Permit #55088; IGSID 167019), an unconventional oil/gas well in Southwest Indiana drilled to explore the lithology, productive capacity, and the fracture complexity of the New Albany Shale. This report provides the core characterization results and aims to meet the growing demand for high quality and comprehensive lithological subsurface data.

The primary objective for this study was to characterize core from the New Albany Shale drilled in an area in Indiana that has high oil/gas potential, utilizing methods not available to most researchers. Computed tomography (CT) and Multi-Sensor Core Logger (MSCL) scanning at NETL in Morgantown, WV provides a means to characterize the core and disseminate the data to the public in several formats; including this report and through NETL's Energy Data eXchange (EDX). The data presented here are potentially useful for various subsequent analyses. However, analysis presented in this report is rather limited as the research objective was not to do a site characterization, but rather to generate the data for others to utilize and to develop a digital representation of the core that could be preserved.

1.1 SITE BACKGROUND

The UW Enterprises LP 1-250512-129 well was drilled in Posey County, Indiana, (UTM X: 437463, UTM Y: 4211907, Zone 16; Township – Range: 5S - 12W) in 2014. Located in the very southwest of Indiana, the UW Enterprises LP 1-250512-129 well is in the southern portion of Illinois Basin as shown in Figure 1. As the target zone of the well, the New Albany Shale in the Illinois Basin is a widely recognized Upper Devonian to Lower Mississippian unit (Strapoć et al., 2010).

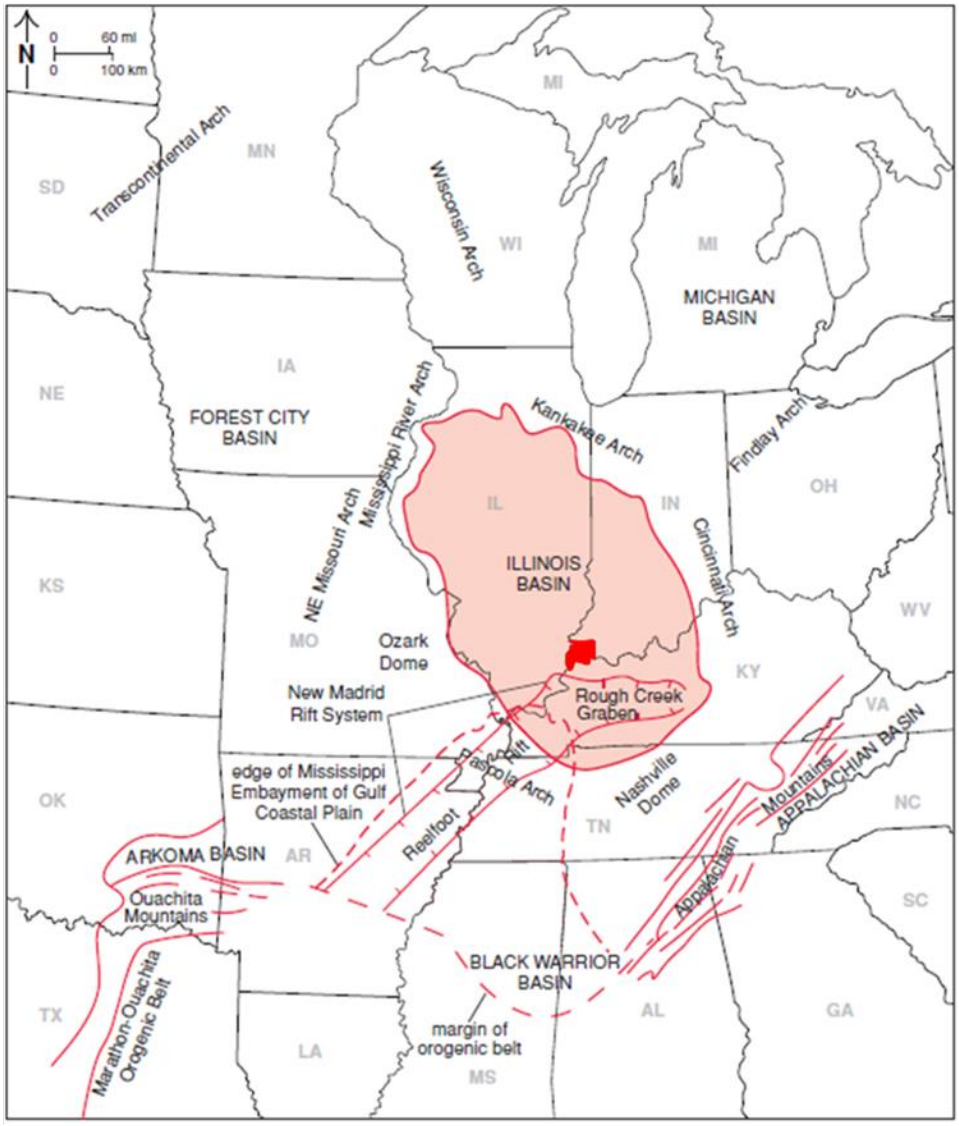

Figure 1: The extent of Illinois Basin and the location of Posey County, Indiana (in red) (modified from Finley, 2014).

2. CORE PHOTOGRAPHS

The UW Enterprises core presented in this study covers the depth range of 4,190–4,466 ft within the New Albany Shale. From 4,190–4,220 ft the core is primarily made up of a light grey calcareous shale with frequent siderite nodules. From 4,220–4,328 ft the core is mainly made up of brown to black organic-rich shale, with pyrite commonly observed at a higher frequency in the deeper depths. Fracturing increases with depth and many fractures are mineralized with calcite.

From 4,328–4,430 ft the core is primarily made up of black to dark grey shale with an increase in calcareous nodules. From 4,430–4,463 ft the core primarily consists of calcareous shale. The interval from 4,463–4,466 ft is mainly represented by light grey calcareous shale and massive, light grey wackestones.

Core photographs are presented to complement the CT imaging and core logging. In the photographs, the top of the core is in the upper, right corner and the core bottom is shown in the bottom, left corner (Figures 2–4).

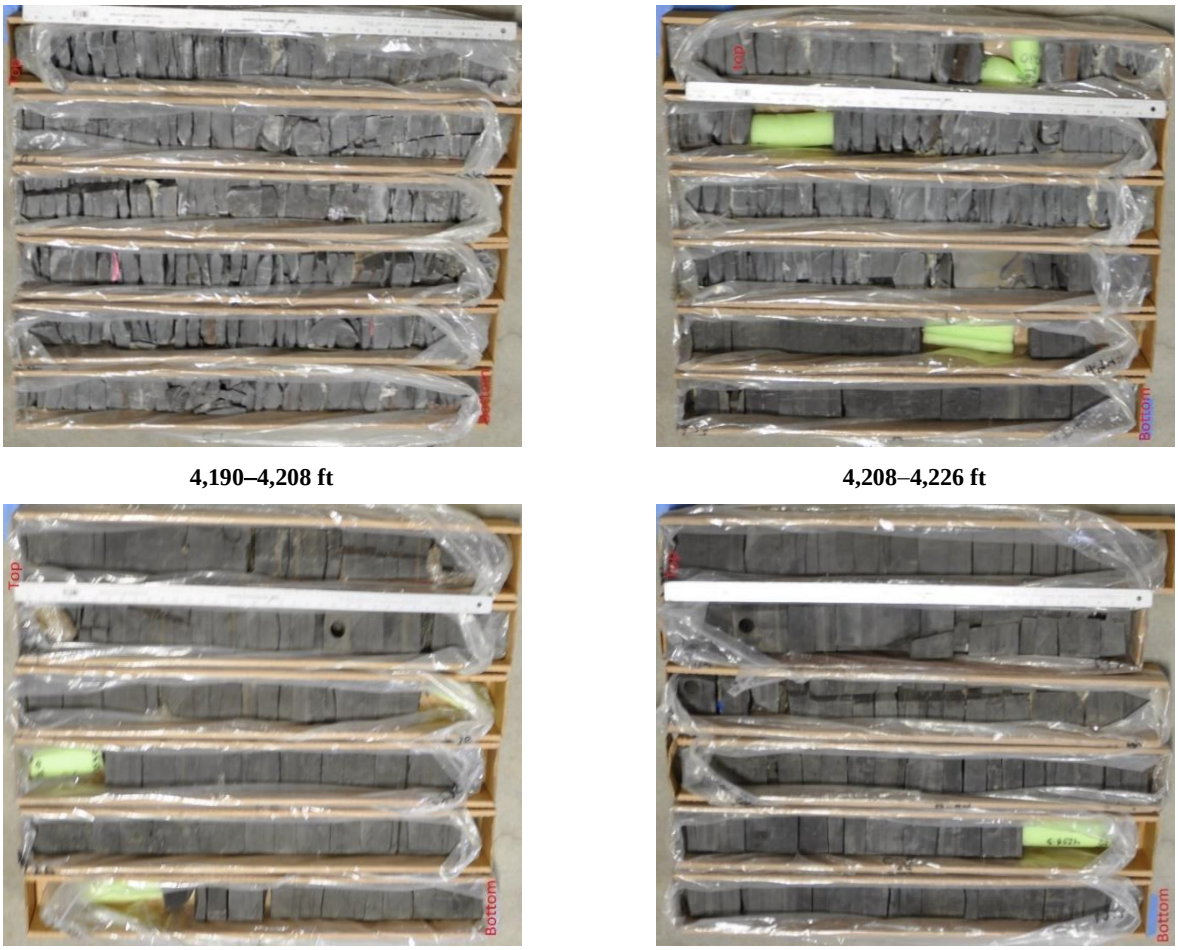

4,190–4,208 ft **4,208–4,226 ft**

4,266–4,244 ft **4,244–4,263 ft**

Figure 2: UW Enterprises LP 1-250512-129 well core photographs from 4,190 to 4,263 ft.

4,263–4,281 ft

4,281–4,299 ft

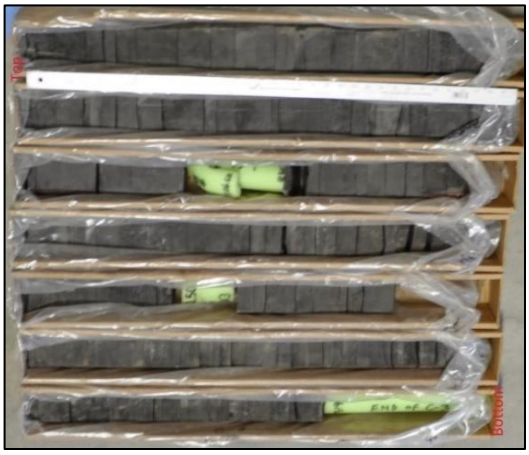

4,299–4,319 ft

4,319–4,340 ft

Figure 3: UW Enterprises LP 1-250512-129 well core photographs from 4,263 to 4,340 ft.

4,340–4,361 ft

4,361–4,382 ft

4,382–4,403 ft

4,403–4,424 ft

4,424–4,445 ft

4,445–4,466 ft

Figure 4: UW Enterprises LP 1-250512-129 well core photographs from 4,340 to 4,466 ft.

3. DATA ACQUISITION AND METHODOLOGY

The core was evaluated using CT scanning, MSCL, and X-ray fluorescence (XRF) spectrometry.

3.1 MEDICAL CT SCANNING

Core scale CT scanning was done with NETL's Toshiba® Aquilion TSX-101A/R medical scanner shown in Figure 5. The medical CT scanner generates images with a resolution in the millimeter range, with scans having voxel resolutions of 0.43 x 0.43 mm in the XY plane and 0.50 mm along the core axis. High energy scans were conducted at a voltage of 135 kV and at a current of 200 mA and these are shown in the following images. Low energy scans were conducted at a voltage of 85 kV and at a current of 200 mA and these were used for dual-energy density calculations. Subsequent processing and combining of stacks were performed to create three-dimensional (3D) volumetric representations of the cores and a two-dimensional (2D) cross-section through the middle of the core samples using ImageJ (Schneider et al., 2012). The variation in greyscale values observed in the images indicate changes in the CT number (CTN) obtained from the CT scans, which is directly proportional to changes in the attenuation and density of the scanned rock. Darker regions are less dense. As can be seen in Section 4.1, filled fractures, open fractures, and changes in bedding structure can all be resolved via careful examination of the CT images. While the medical CT scanner was not used for detailed characterization in this study, it allowed for non-destructive bulk characterization of the core.

Figure 5: Toshiba® Aquilion™ Multislice Helical CT Scanner at NETL used for core analysis.

3.2 INDUSTRIAL CT SCANNING

High-resolution CT scans were performed on intervals of interest using the North Star Imagining Inc. M-5000® Industrial CT System shown in Figure 6. The system is used to obtain higher resolution scans resolving finer features than the medical scans.

The scans were performed at 185 kV and 200 μA to provide resolutions between 55 and 58 μm^3. Scans consisted of 1,440 radiographs, or at every 0.25°. Radiographs are comprised of 10 images averaged with a 5 second acquisition for each image to ensure sufficient image contrast. Industrial CT scans of select depths from the UW Enterprises core are shown in Section 4.2.

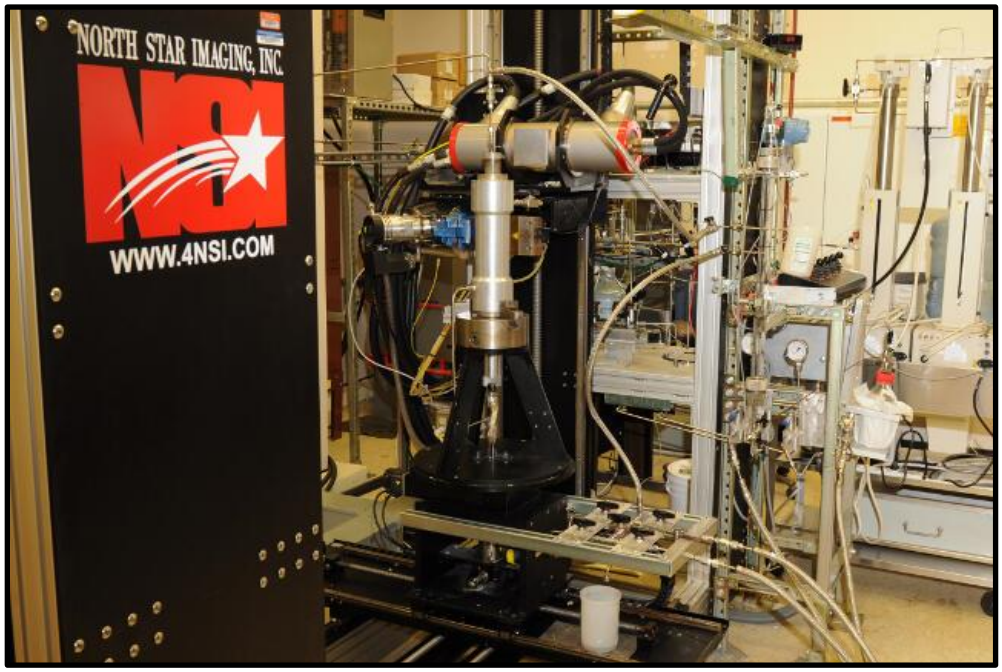

Figure 6: North Star Imaging Inc. M-5000 ® Industrial CT Scanner at NETL used for core analysis.

3.3 MICRO-CT SCANNING

Micro-CT scanning was performed using a ZEISS Xradia MicroXCT-*400* (Xradia) scanner. The Xradia system has the highest resolution of all the CT scanners at NETL and scans samples sized from sub-mm to 25 mm. The scanner provides detailed image data that can be used to infer porosity, mineralogy, and structure. The scan provided in Section 4.2.2 was performed at 150 kV and 9.8W providing a voxel resolution of 1.8 μm^3 over 5 scans that were stitched together using ImageJ. Scans consisted of 3,601 radiographs over 180 degrees, or at every 0.05°.

3.4 CORE LOGGING

Geophysical measurements of P-wave travel time, magnetic susceptibility, and attenuated gamma counts were obtained with a Geotek® MSCL system on competent sections of the core (see Section 4.3). Additionally, the system was used to measure bulk elemental chemistry with a built-in, portable XRF spectrometer.

The compiled core logs were scaled to fit on single pages for rapid review of the combined data from the medical CT scans and MSCL, including XRF readings.

3.4.1 Magnetic Susceptibility

Magnetic susceptibility is a measure of the degree of magnetization in a sample. The sample is exposed to an external magnetic field and magnetic susceptibility is the measured magnetic response to that field:

$$J = kH$$

Where *J* is the magnetic response (per unit volume), *k* is volume susceptibility, and *H* is an external magnetic field. The measurement unit is dimensionless (abbreviated simply as SI). All materials have magnetic susceptibility (Hunts et al., 1995).

Magnetic susceptibility is measured using the Bartington point sensor, where a 1 cm diameter, low intensity (8.0 A/m RMS), non-sensitive, alternating magnetic field (2 kHz) is generated for 10 seconds. To minimize any potential drift in the oscillating field, the point sensor is zeroed at the beginning and end of the sample, as well as, after every fifth measurement. The point sensor, due to the small field, is limited in whole core measurements and additionally is temperature-dependent (Geotek Ltd. Multi-Sensor Core Logger Manual, Version 05-10).

Table 1: Magnetic Susceptibility Values for Common Minerals (Hunts et al., 1995)

Mineral	X (*10^{-6}) SI
Water	9
Calcite	-7.5 to -39
Halite, Gypsum	-10 to -60
Illite, Montmorillonite	330 to 410
Pyrite	5 to 3,500
Haematite	500 to 40,000
Magnetite	1,000,000 to 5,700,000

3.4.2 P-wave Velocity

The P-wave velocity (*v*) measurements were conducted to determine the acoustic impedance of a geologic sample using compressional waves. Acoustic impedance (Z) is a measure of a material's ability to transmit vibrations, which is directly proportional to its density and/or degree of consolidation.

$$Z = v * \rho_B$$

For example, air has low acoustic impedance with a wave speed of 330 m/s, while granite has high acoustic impedance with a wave speed of more than 5,000 m/s. These measurements can be used

as proxies for seismic reflection coefficients and can inform field data when conducting seismic surveys.

The software associated with the MSCL measures the travel time of the pulse with a 50 ns resolution and has an absolute accuracy of ± 3 m/s with a resolution of 1.5 m/s (Geotek Ltd., 2010).

3.4.3 Gamma Density

Gamma density is acquired by subjecting the sample to gamma radiation and then measuring the attenuation of that radiation. The attenuation is directly proportional to the density of the sample and is acquired by measuring the difference between radiation energy at the emission source and after it passes through the sample. Specifically, the MSCL software calculates the bulk density, ρ, by using the following equation:

$$\rho = \left(\frac{1}{\mu d}\right) \ln\left(\frac{I_o}{I}\right)$$

Where μ is the Compton attenuation coefficient, d is the sample thickness, I_o is the source intensity, and I is the measured intensity.

3.5 X-RAY FLUORESCENCE SPECTROMETRY

In addition to the geophysical measurements, a portable handheld Olympus Vanta M Series X-Ray Fluorescence Spectrometer was used to measure relative elemental abundances of aggregated "light elements" up to and including sodium, and various "heavy elements" which were measured individually. Elemental abundances are reported in ppm relative to the total elemental composition (i.e., the total XRF counts).

The XRF spectrometer measures elemental abundances by subjecting the sample to X-ray photons. The high energy of the photons displaces inner orbital electrons in the respective elements. The vacancies in the lower orbitals cause outer orbital electrons to "fall" into lower orbits to satisfy the disturbed electron configuration. The substitution into lower orbitals causes a release of a secondary X-ray photon, which has an energy associated with a specific element. These relative and element specific energy emissions can then be used to determine bulk elemental composition.

The Olympus Vanta M Series X-Ray Fluorescence Spectrometer used a "GeoChem(3-beam) Mode" was run at 30.48 cm (1 ft) resolution for 120 s exposure time analysis (40 s per beam). The GeoChem(3-beam) Mode utilizes a 3-beam analysis that resolves major (Mg, Al, Si, P, S, Fe, K, Ca, and Ti), minor (V, Cu, Ni, Cr, Mn, Ba, Sr, and Pb), and trace elements (Co, Zn, As, Zr, Mo, Ag, Cd, Sn, Sb, Hf, W, Th, U, and Bi) and some rare earth elements (Y, Ce, La, Pr, and Nd). The system also resolves an aggregated "light element" (H to Na).

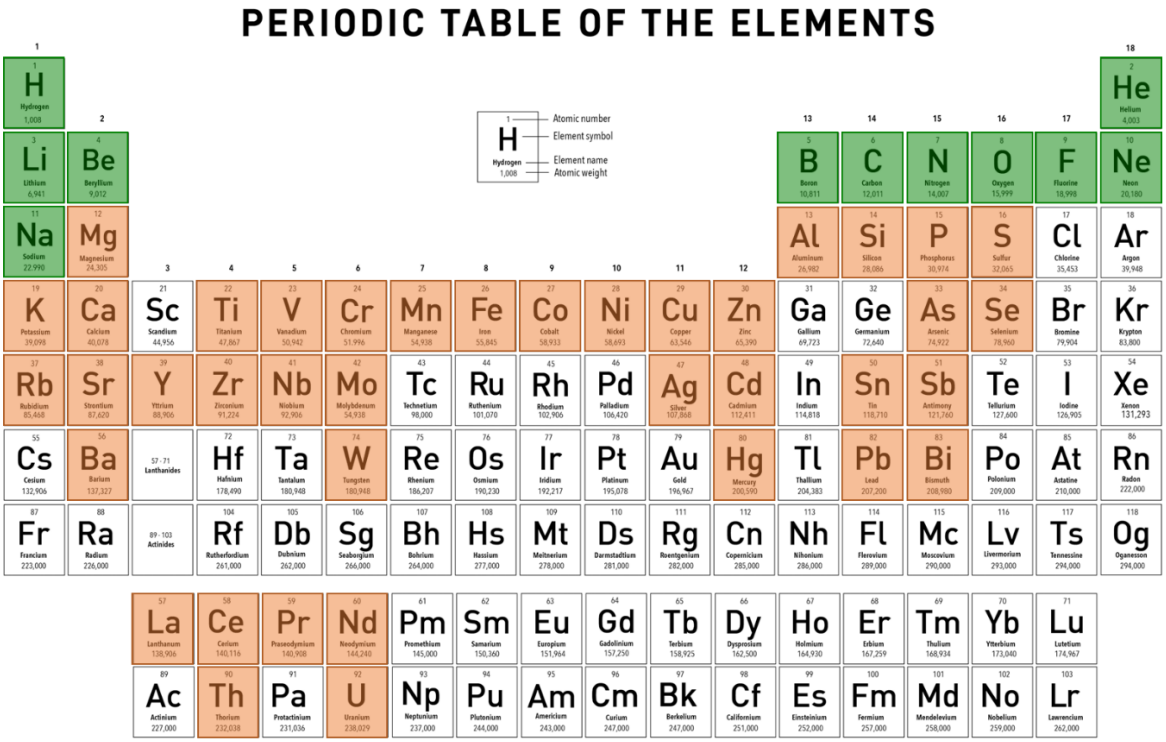

Figure 7: Periodic table showing elements measurable by the Olympus Vanta M Series X-Ray Fluorescence Spectrometer using the "GeoChem(3-beam)" mode.

3.6 DATA COMPILATION

Strater® by Golden Software® was used to compile the medical CT data into a series of logs. The data used to generate these logs can be accessed from NETL's EDX online system using the following link: https://edx.netl.doe.gov/dataset/uw-enterprises.

4. RESULTS

Processed 2D slices of the medical CT scans through the cores are shown in Figures 9–27.

4.1 MEDICAL CT SCANS

As was discussed previously, the variation in greyscale values observed in the medical CT images indicates changes in the CT number obtained, which is directly proportional to changes in the attenuation and density of the scanned rock (i.e., darker regions are less dense). Detailed information in logbooks and photographs of the core were used to confirm the locations of missing core and depths, if needed.

4.1.1 XZ Planes

A 2D image through the center of each core can be found in Figures 9–27. These are referred to as XZ planes with the coordinates that are shown in Figure 8. There is a 2 cm scale bar shown in these images; the retrieved core has a diameter of 4 in (10.1 cm) for reference. The labels below each 2D XZ plane in Figures 9–27 are the depth range of each boxed core section; the full range of core lengths shown in each figure is listed in the figure captions. The greyscale range was maintained to a range of 750 to 3,250 on a 16-bit scale for all core CT images.

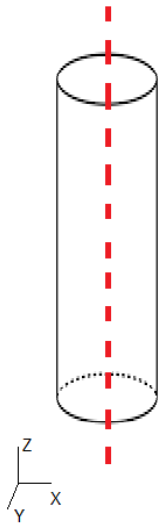

Figure 8: Schematic of the XZ isolated plane through the vertical center of the medical CT scans.

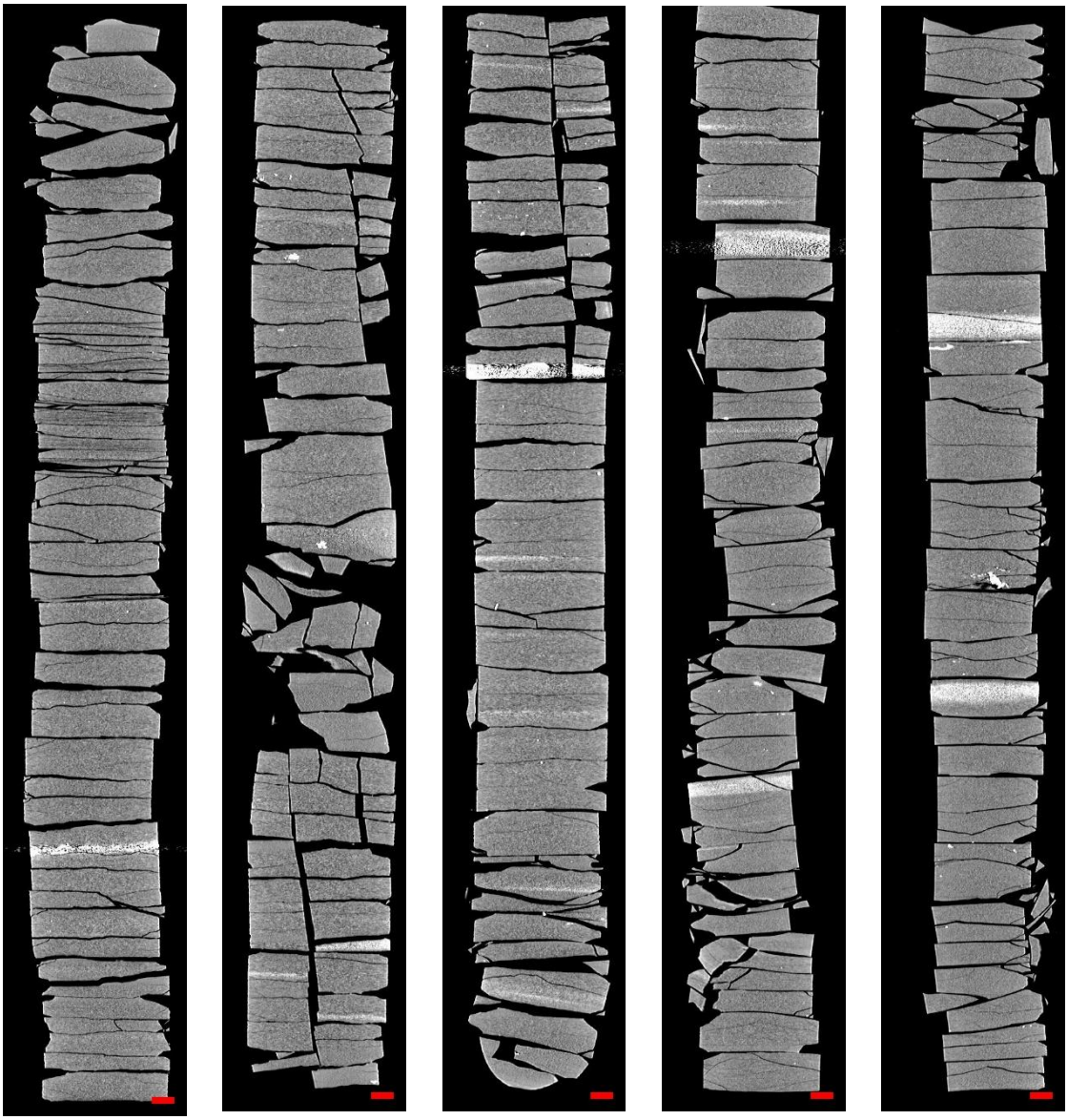

4,190–4,193 ft **4,193–4,196 ft** **4,196–4,199 ft** **4,199–4,202 ft** **4,202–4,205 ft**

Figure 9: 2D isolated planes through the vertical center of the medical CT scans of the UW Enterprises LP 1-250512-129 well core from 4,190 to 4,205 ft.

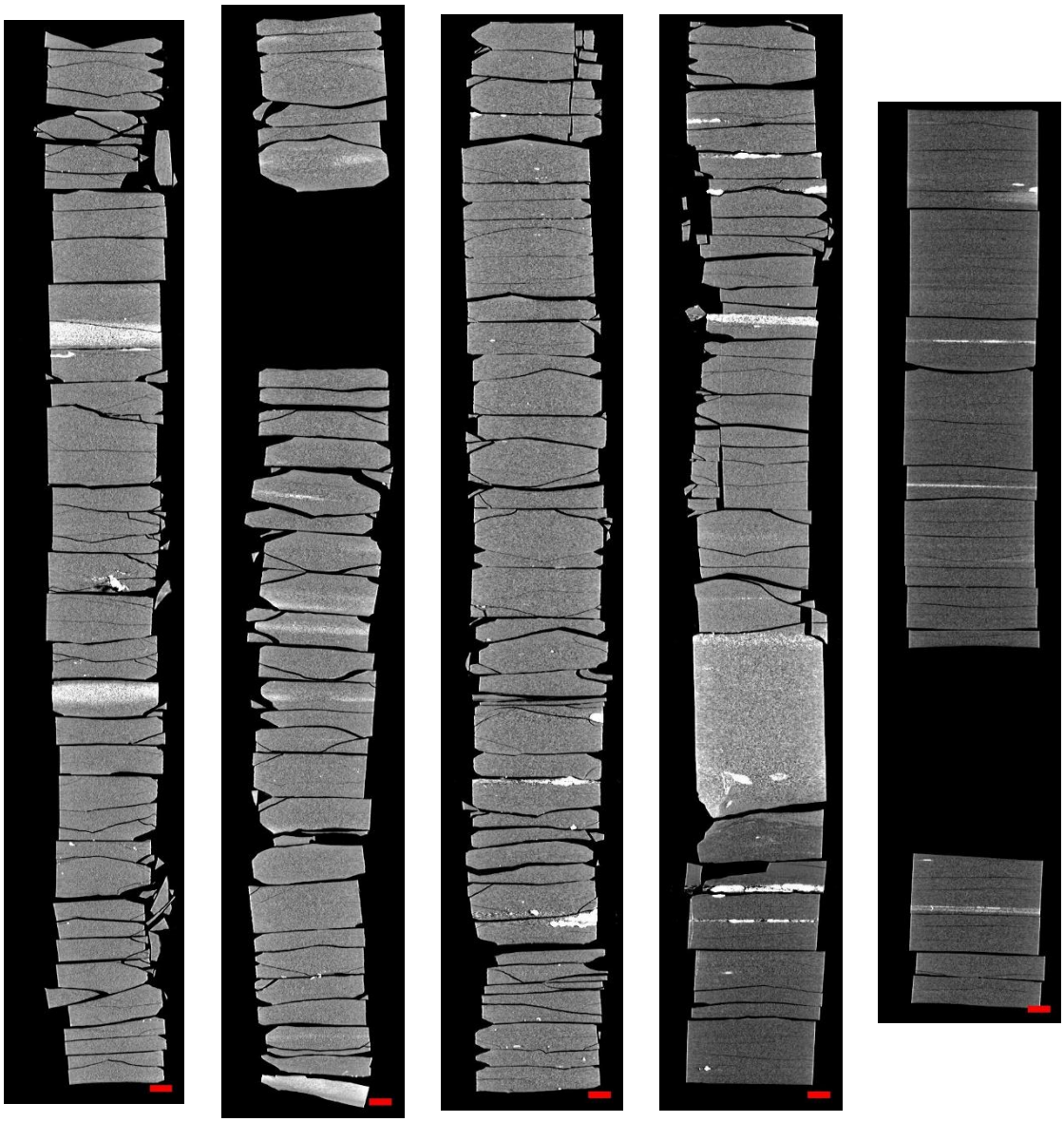

4,205–4,208 ft **4,211–4,214 ft** **4,214–4,217 ft** **4,217–4,220 ft** **4,220–4,223 ft**

Figure 10: 2D isolated planes through the vertical center of the medical CT scans of the UW Enterprises LP 1-250512-129 well core from 4,205 to 4,223 ft.

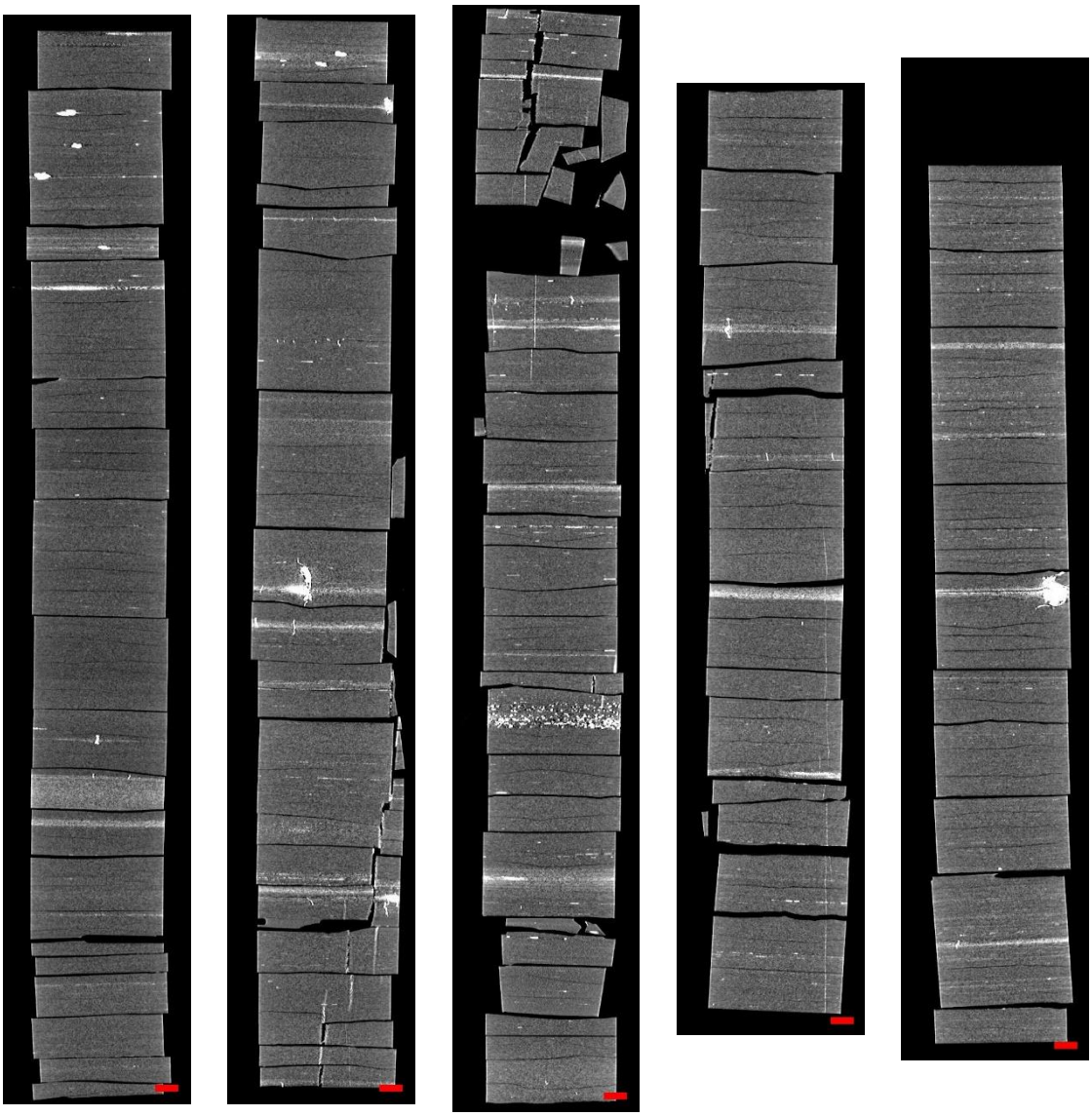

4,223–4,226 ft **4,226–4,229 ft** **4,229–4,232 ft** **4,232–4,235 ft** **4,235–4,238 ft**

Figure 11: 2D isolated planes through the vertical center of the medical CT scans of the UW Enterprises LP 1-250512-129 well core from 4,223 to 4,238 ft.

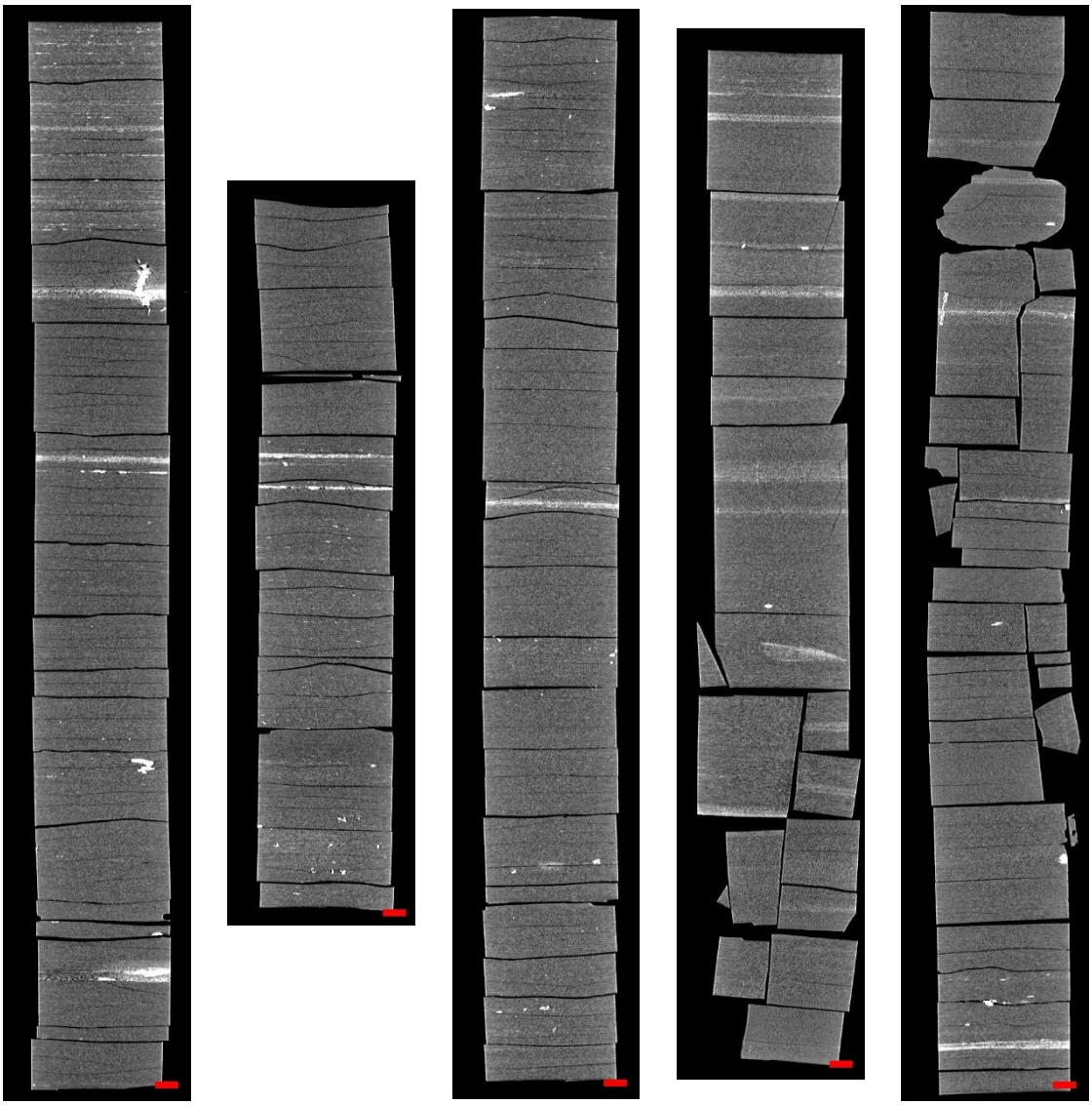

Figure 12: 2D isolated planes through the vertical center of the medical CT scans of the UW Enterprises LP 1-250512-129 well core from 4,238 to 4,253 ft.

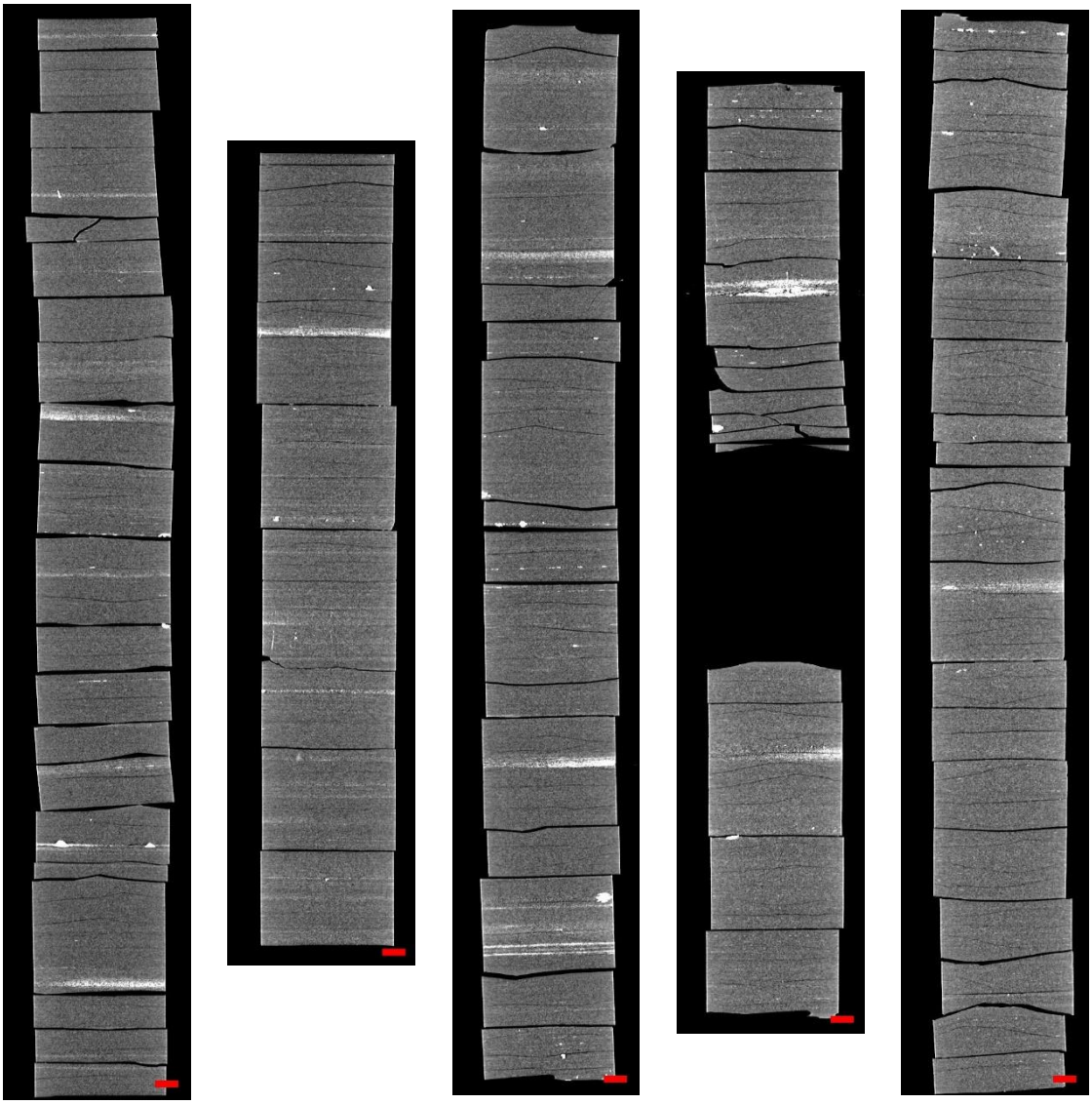

4,253–4,256 ft **4,256–4,258 ft** **4,260–4,263 ft** **4,263–4,266 ft** **4,266–4,269 ft**

Figure 13: 2D isolated planes through the vertical center of the medical CT scans of the UW Enterprises LP 1-250512-129 well core from 4,253 to 4,269 ft.

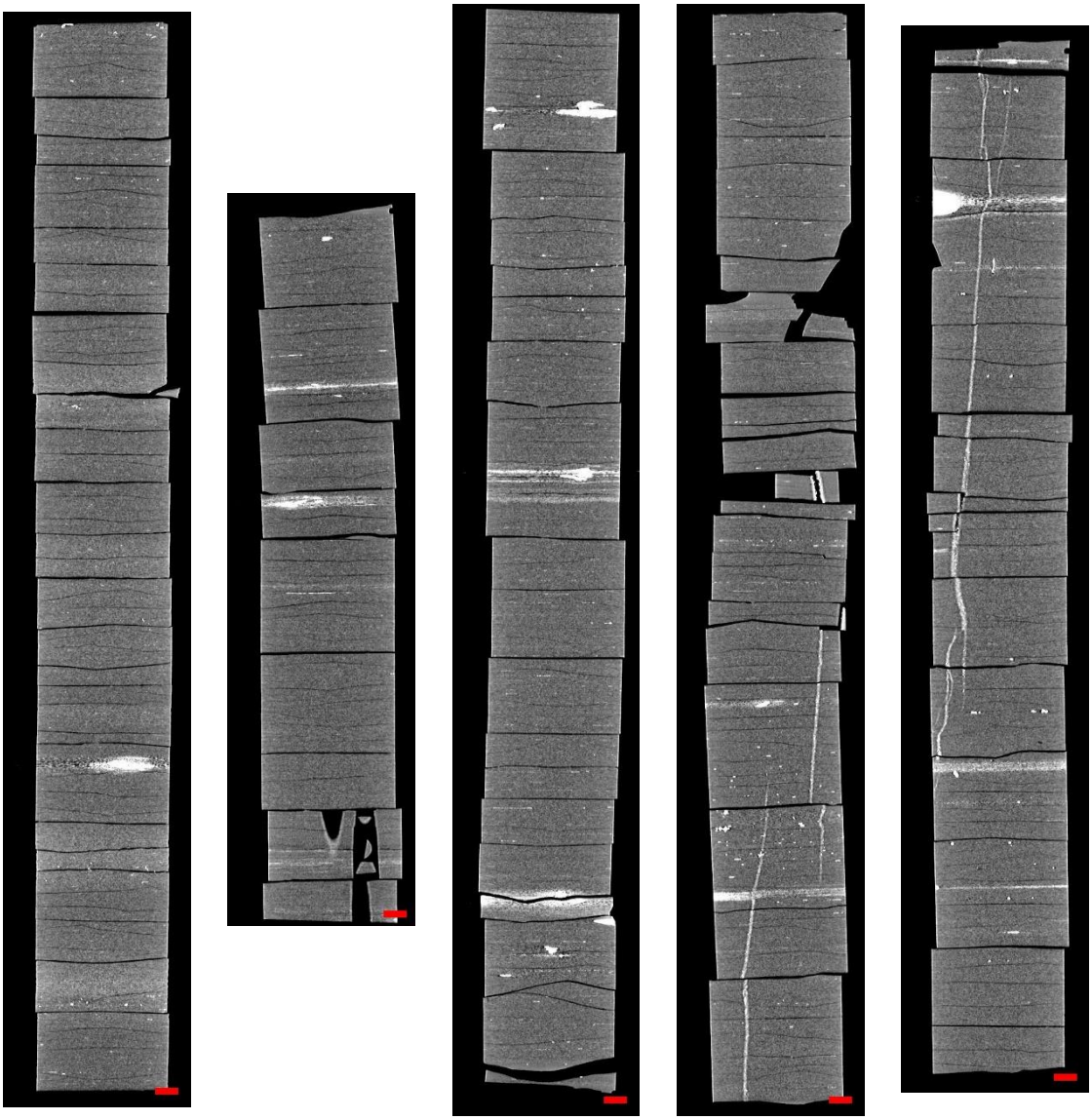

4,269–4,272 ft **4,272–4,275 ft** **4,275–4,278 ft** **4,278–4,281 ft** **4,281–4,284 ft**

Figure 14: 2D isolated planes through the vertical center of the medical CT scans of the UW Enterprises LP 1-250512-129 well core from 4,269 to 4,284 ft.

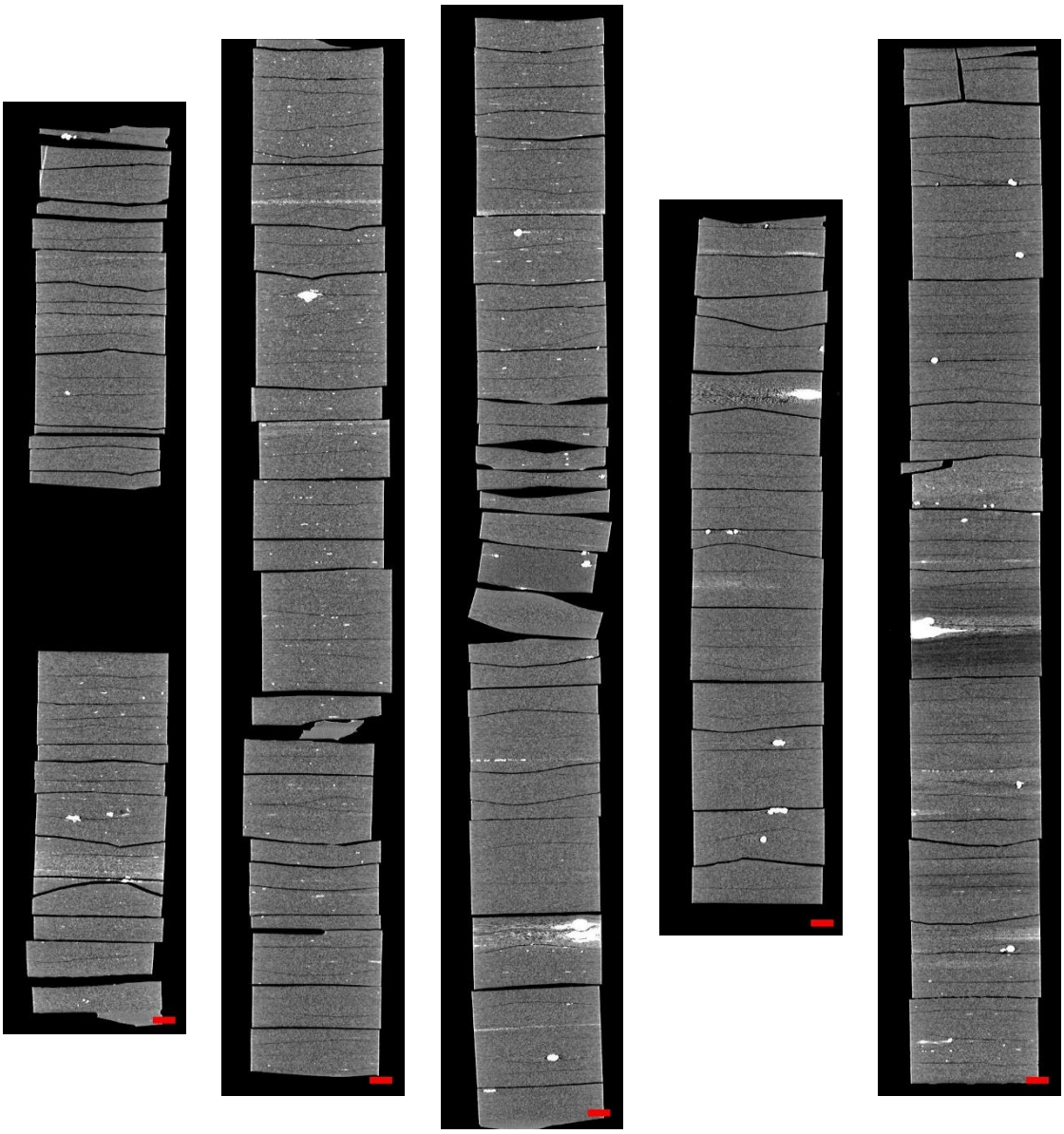

4,284–4,287 ft **4,287–4,290 ft** **4,290–4,293 ft** **4,293–4,296 ft** **4,296–4,299 ft**

Figure 15: 2D isolated planes through the vertical center of the medical CT scans of the UW Enterprises LP 1-250512-129 well core from 4,284 to 4,299 ft.

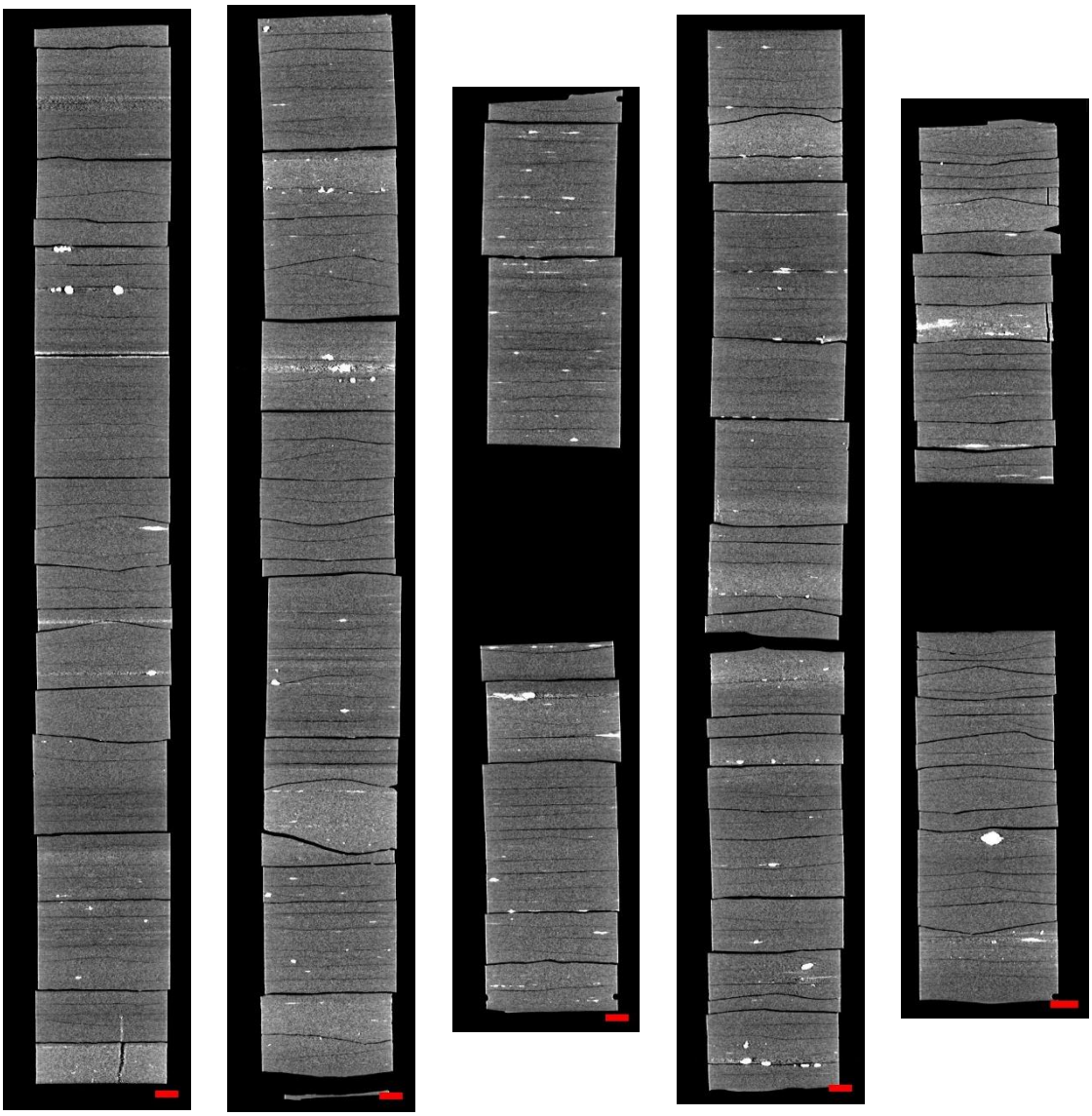

Figure 16: 2D isolated planes through the vertical center of the medical CT scans of the UW Enterprises LP 1-250512-129 well core from 4,299 to 4,314 ft.

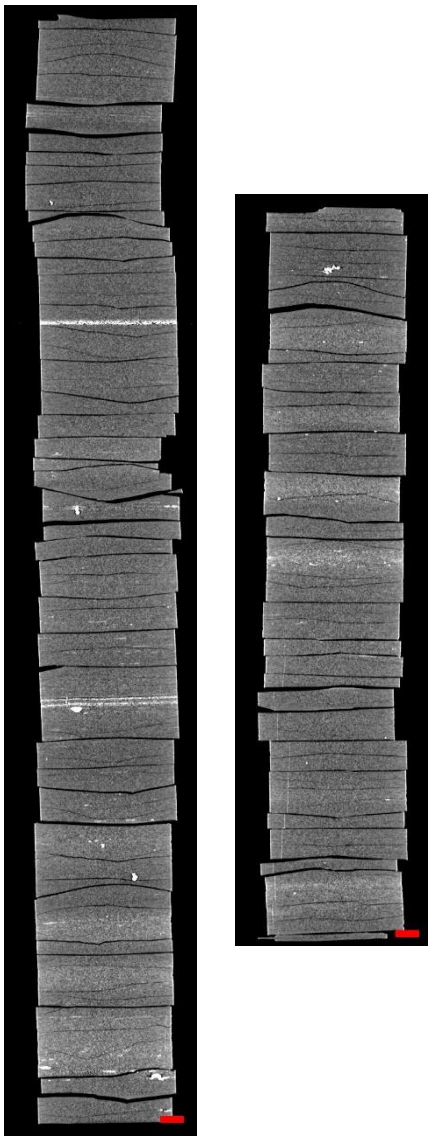

4,314–4,317 ft **4,317–4,319 ft**

Figure 17: 2D isolated planes through the vertical center of the medical CT scans of the UW Enterprises LP 1-250512-129 well core from 4,314 to 4,319 ft.

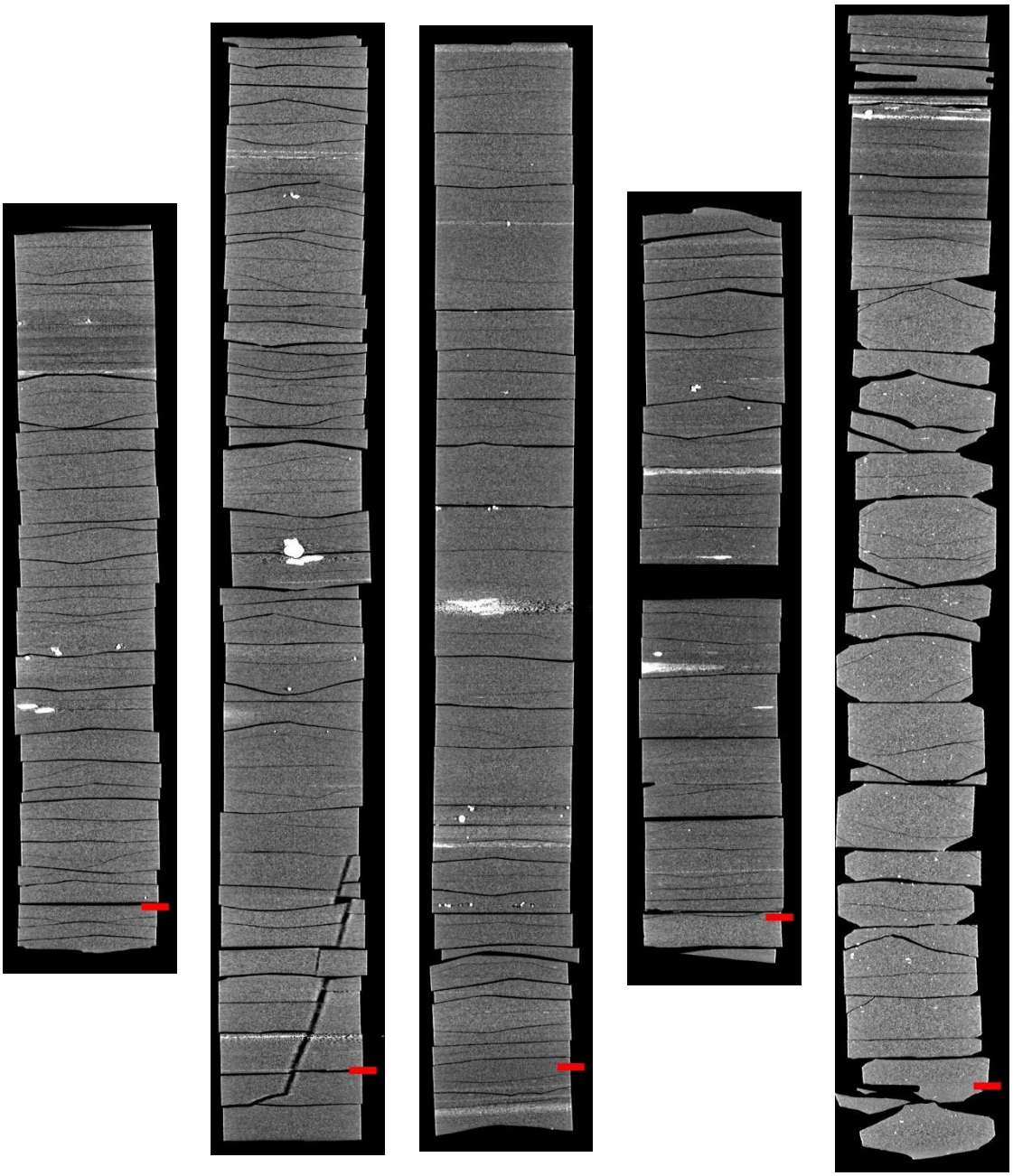

Figure 18: 2D isolated planes through the vertical center of the medical CT scans of the UW Enterprises LP 1-250512-129 well core from 4,322 to 4,337 ft.

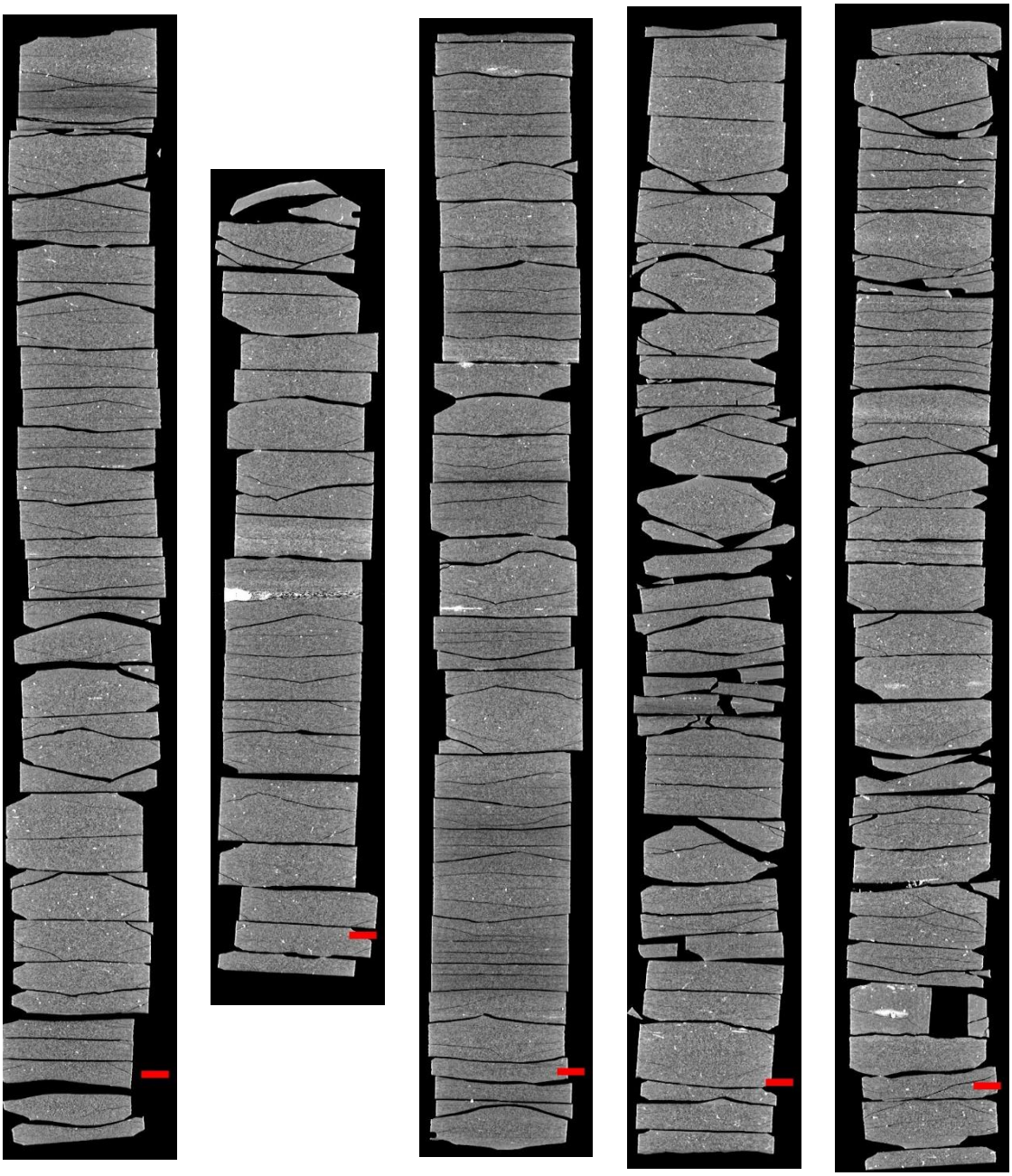

Figure 19: 2D isolated planes through the vertical center of the medical CT scans of the UW Enterprises LP 1-250512-129 well core from 4,337 to 4,352 ft.

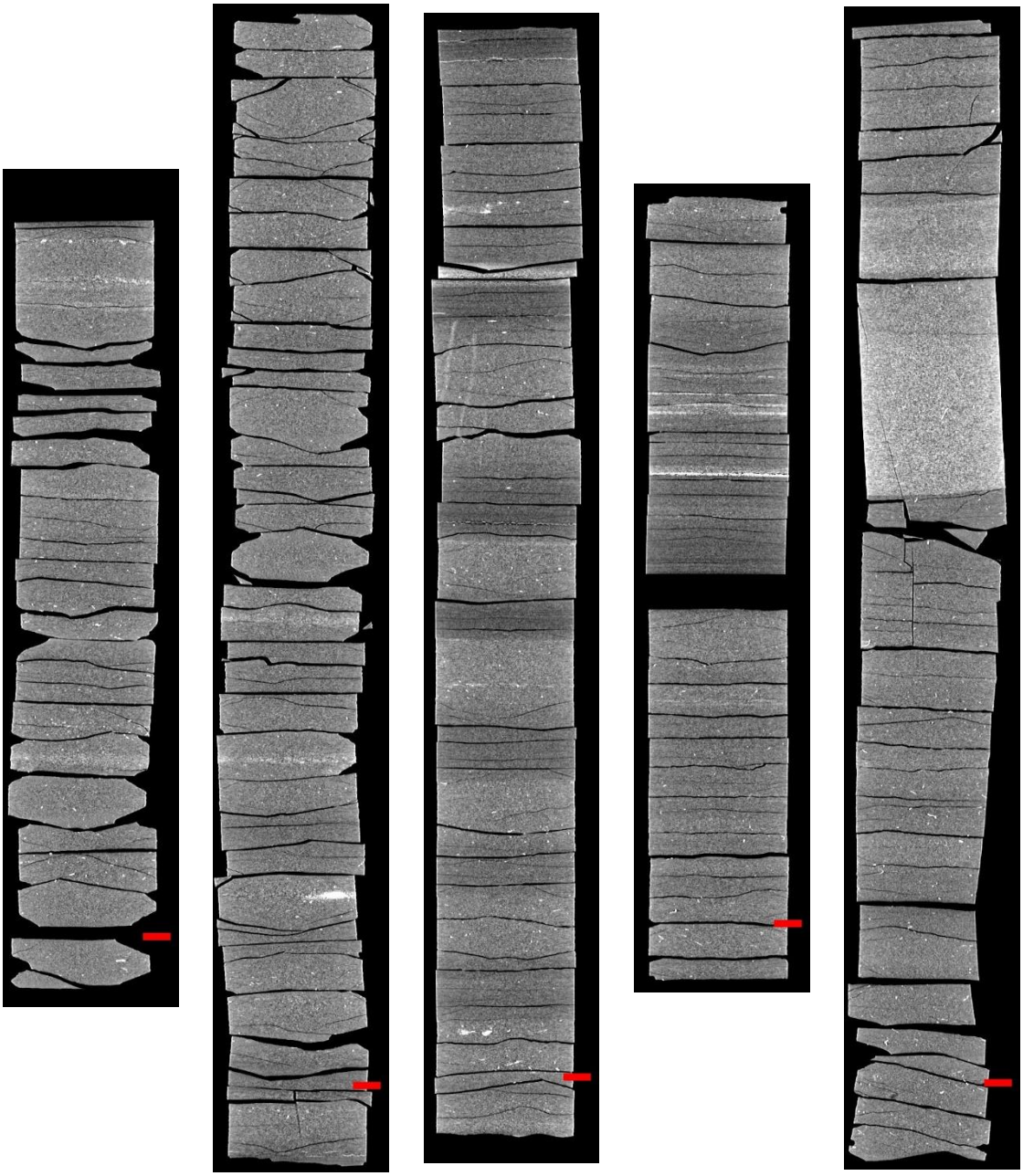

Figure 20: 2D isolated planes through the vertical center of the medical CT scans of the UW Enterprises LP 1-250512-129 well core from 4,352 to 4,367 ft.

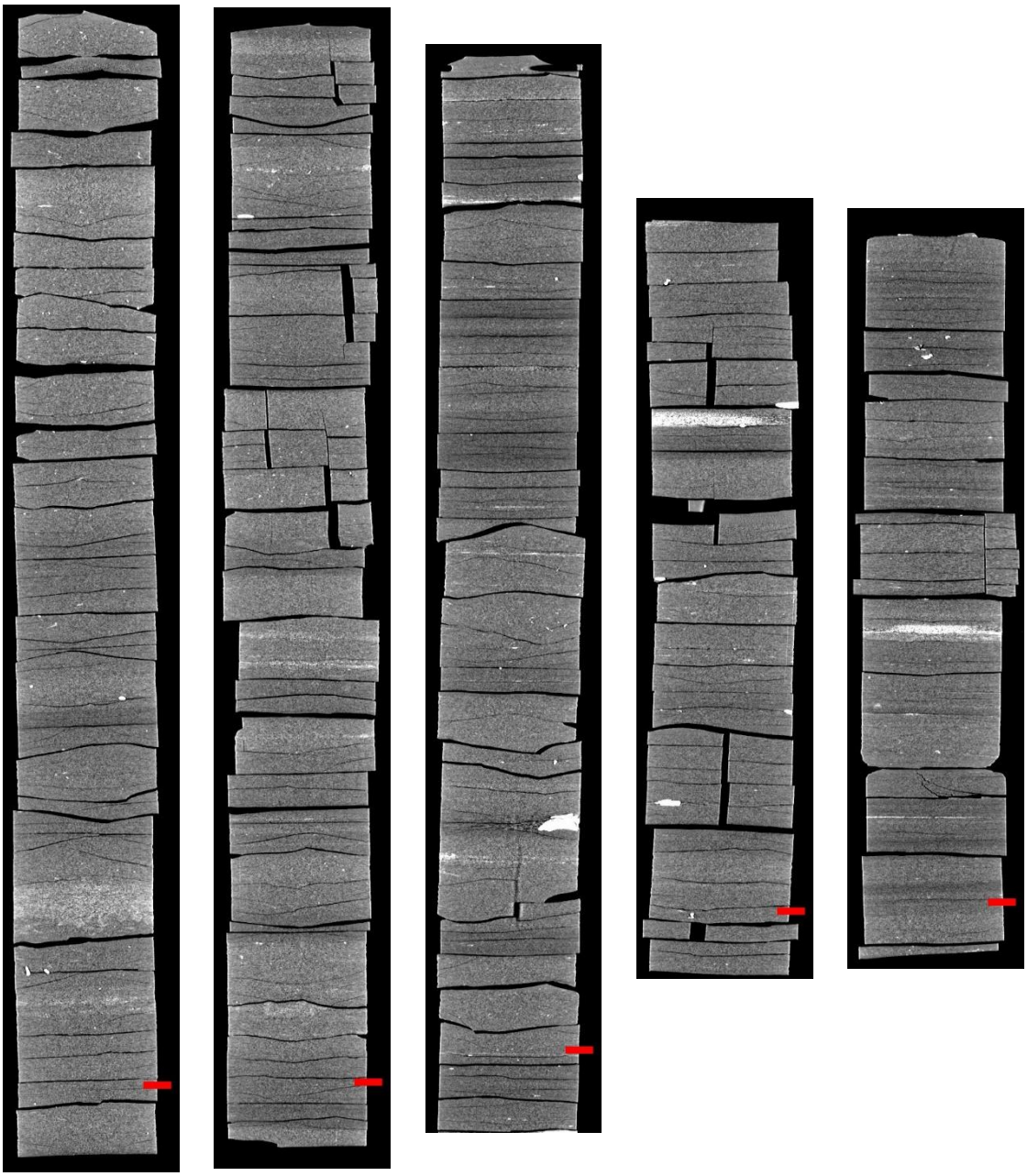

Figure 21: 2D isolated planes through the vertical center of the medical CT scans of the UW Enterprises LP 1-250512-129 well core from 4,367 to 4,381 ft.

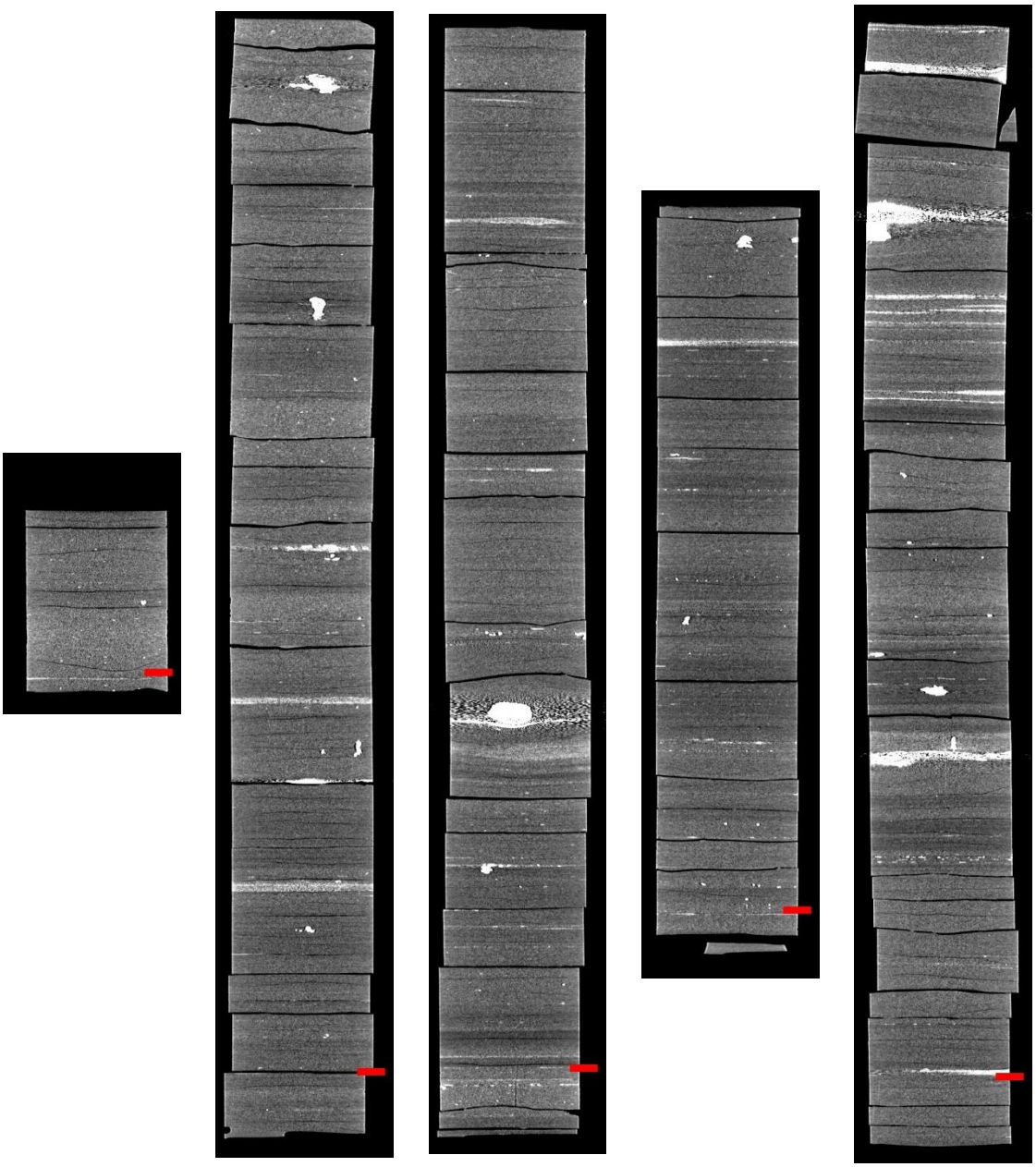

4,381–4,382 ft **4,382–4,385 ft** **4,385–4,388 ft** **4,388–4,391 ft** **4,391–4,394 ft**

Figure 22: 2D isolated planes through the vertical center of the medical CT scans of the UW Enterprises LP 1-250512-129 well core from 4,381 to 4,394 ft.

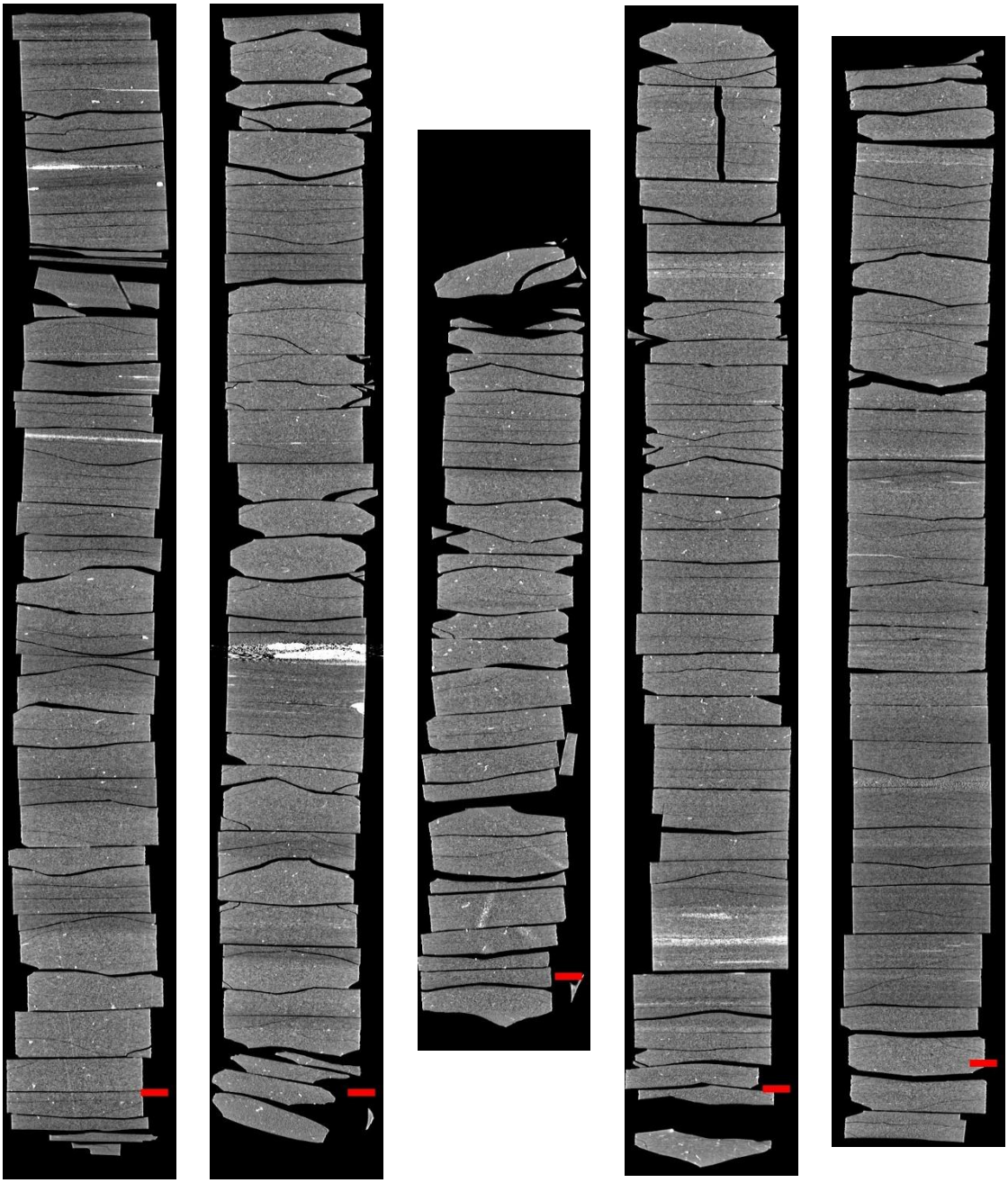

4,394–4,397 ft **4,397–4,400 ft** **4,400–4,403 ft** **4,403–4,406 ft** **4,406–4,409 ft**

Figure 23: 2D isolated planes through the vertical center of the medical CT scans of the UW Enterprises LP 1-250512-129 well core from 4,394 to 4,409 ft.

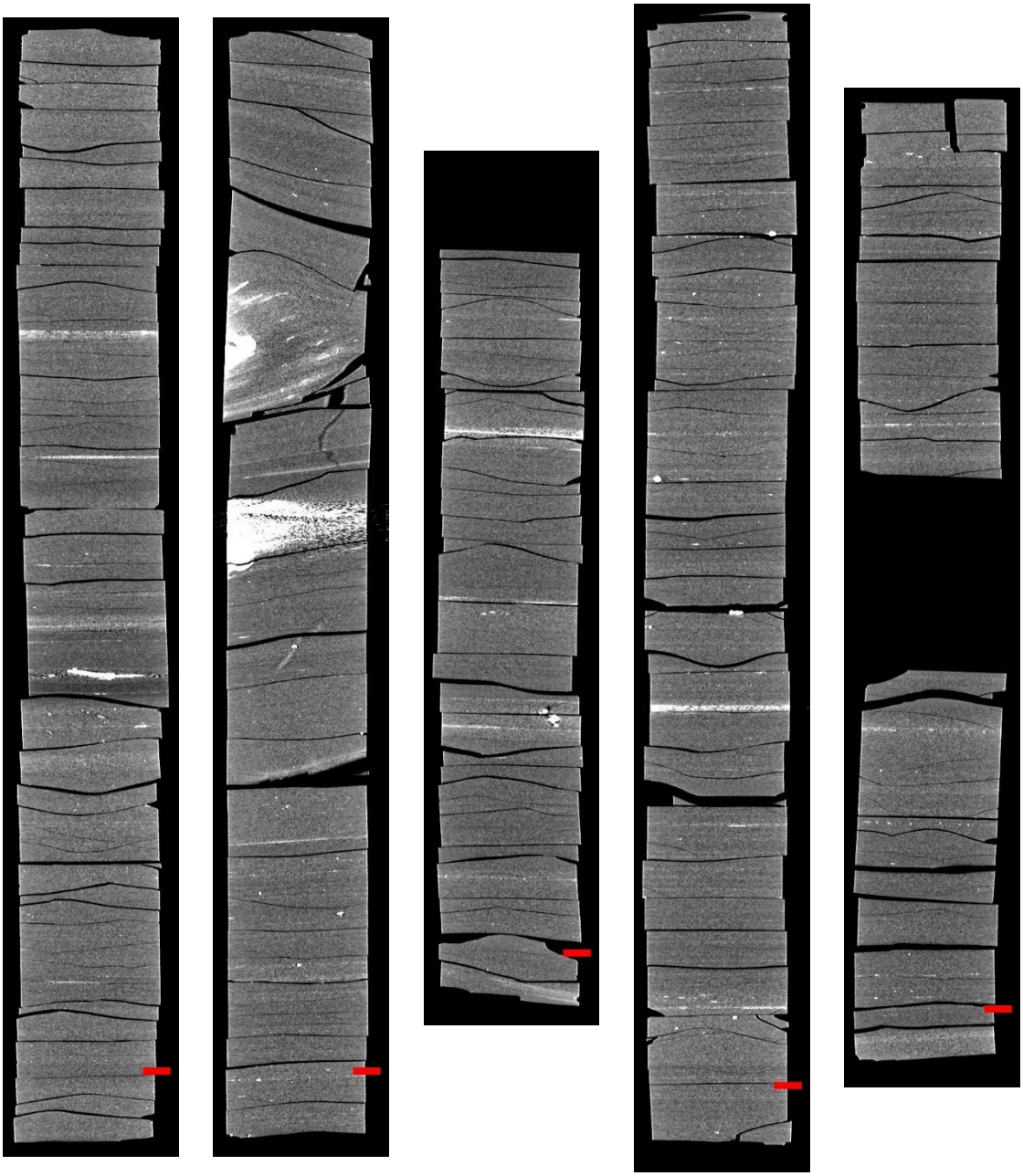

Figure 24: 2D isolated planes through the vertical center of the medical CT scans of the UW Enterprises LP 1-250512-129 well core from 4,409 to 4,424 ft.

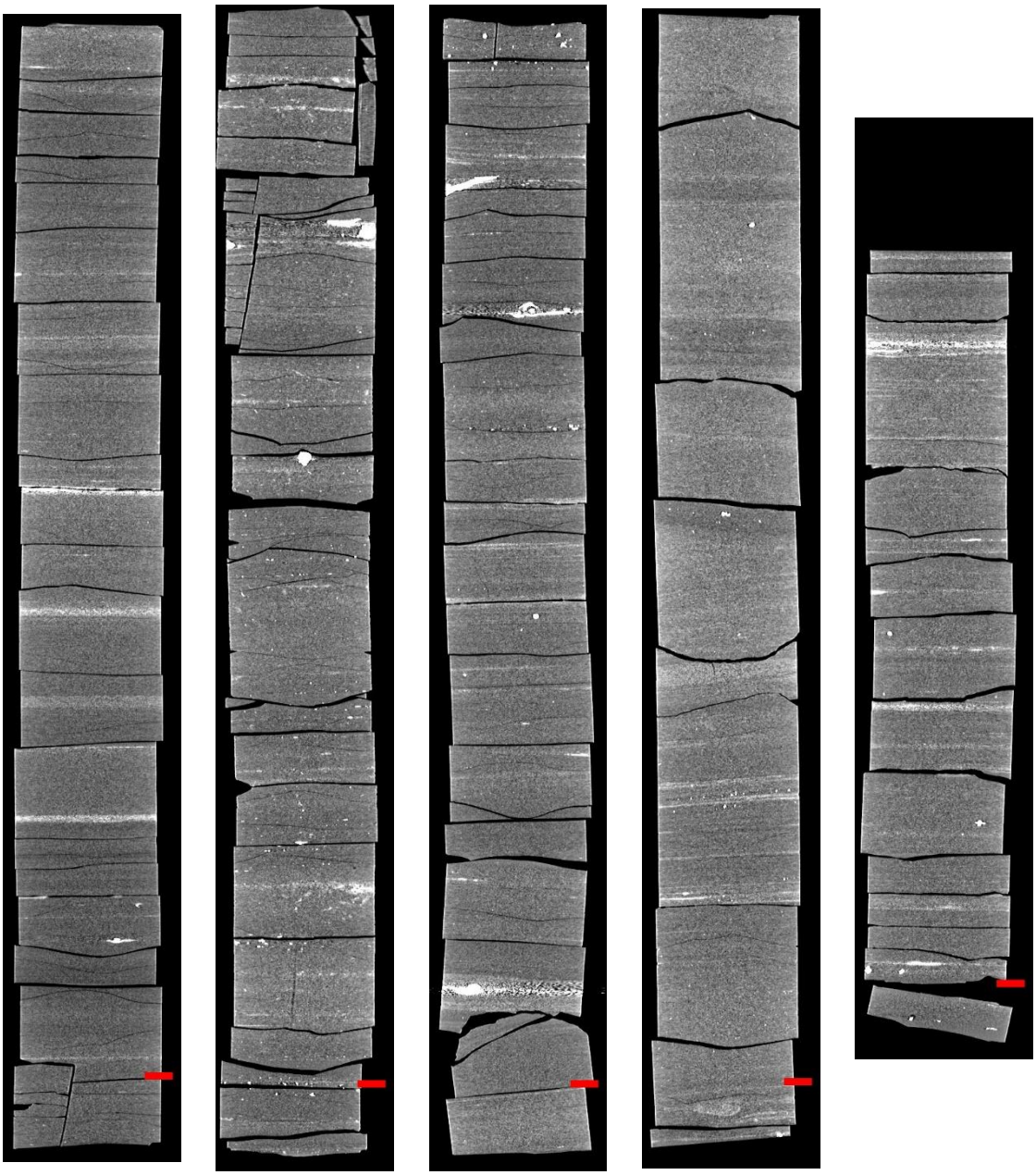

4,424–4,427 ft **4,427–4,430 ft** **4,430–4,433 ft** **4,433–4,436 ft** **4,436–4,439 ft**

Figure 25: 2D isolated planes through the vertical center of the medical CT scans of the UW Enterprises LP 1-250512-129 well core from 4,424 to 4,439 ft.

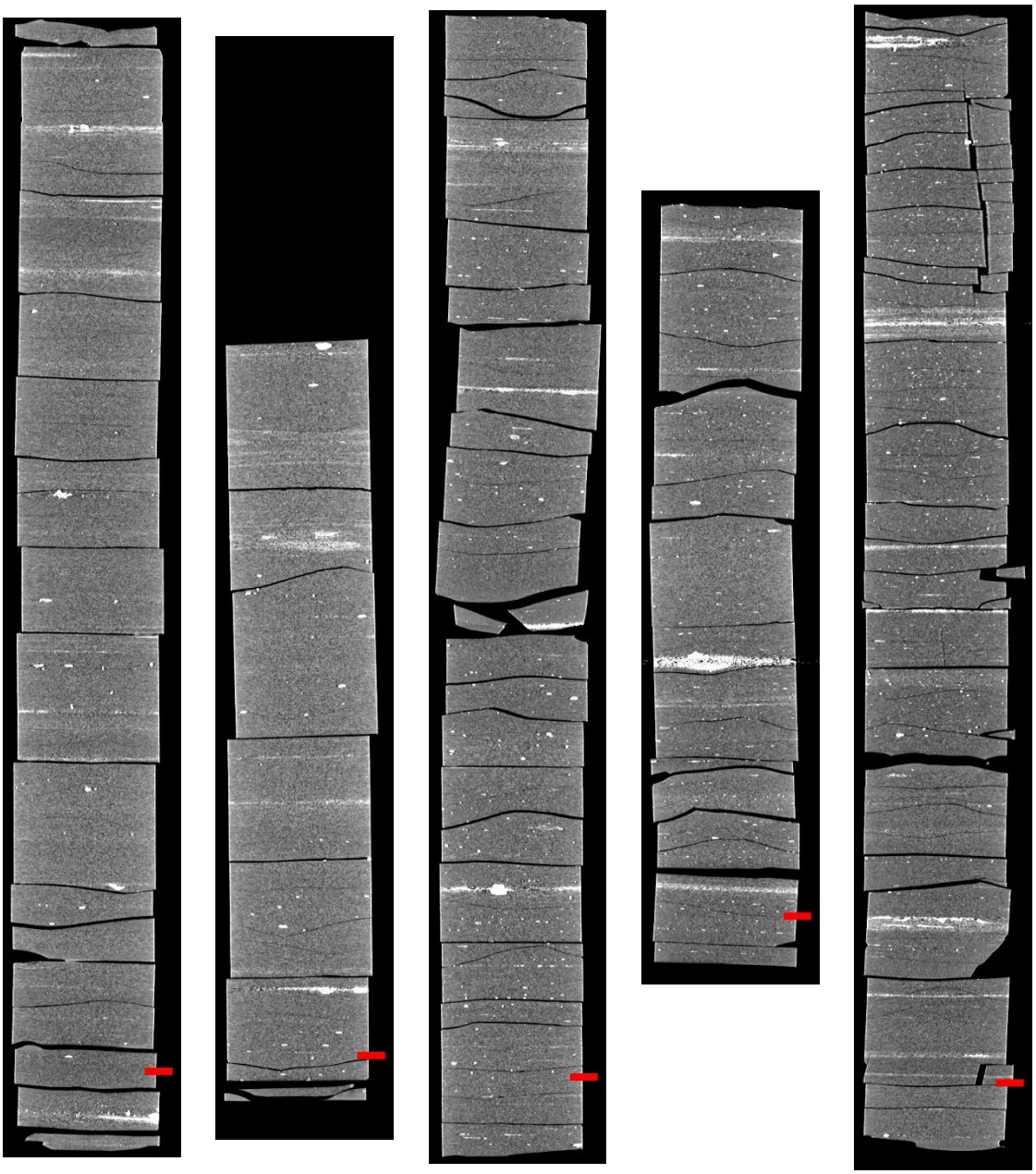

Figure 26: 2D isolated planes through the vertical center of the medical CT scans of the UW Enterprises LP 1-250512-129 well core from 4,439 to 4,454 ft.

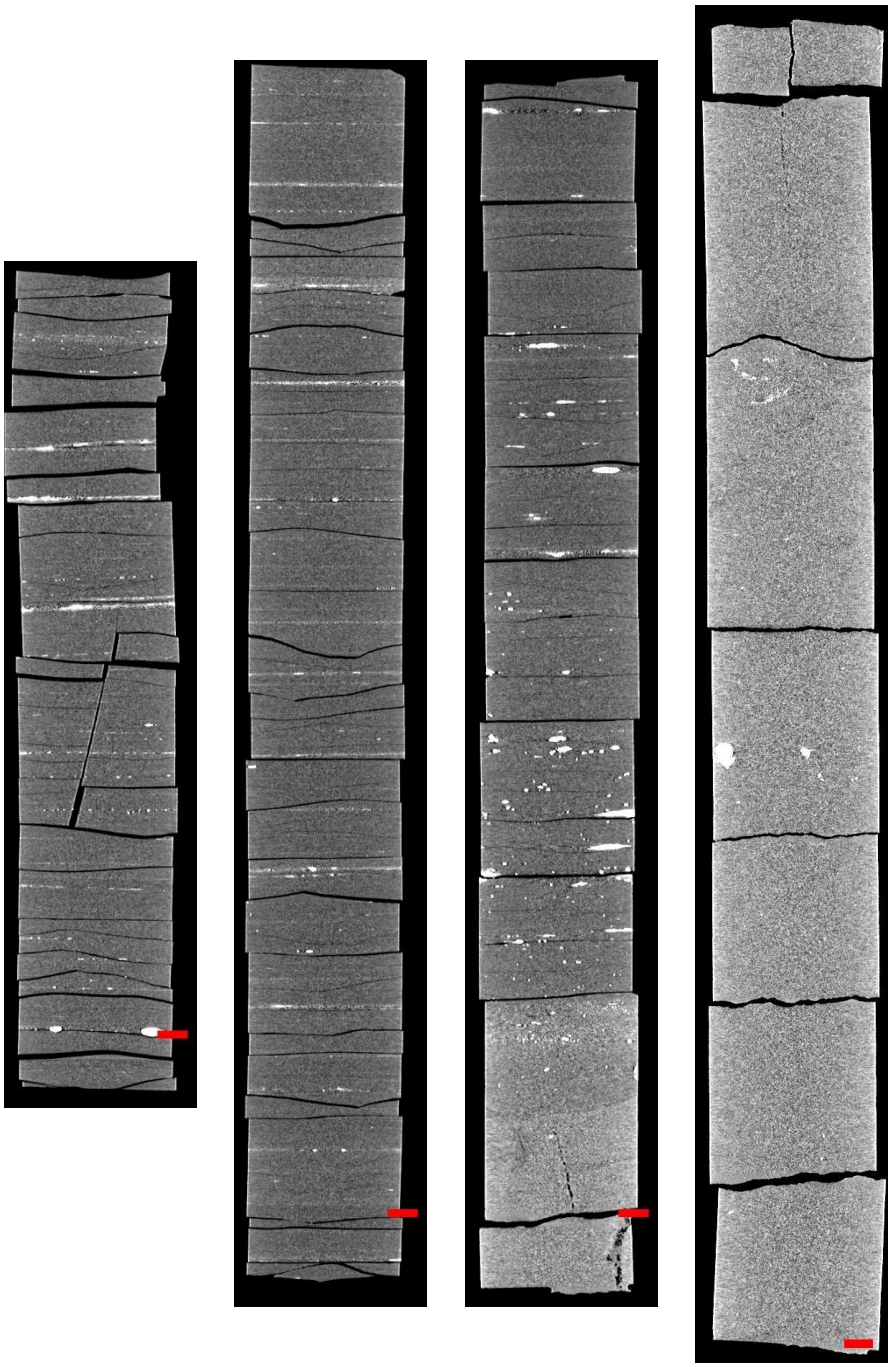

Figure 27: 2D isolated planes through the vertical center of the medical CT scans of the UW Enterprises LP 1-250512-129 well core from 4,454 to 4,466 ft.

4.2 ADDITIONAL CT DATA

Additional CT data can be accessed from NETL's EDX online system using the following link: https://edx.netl.doe.gov/dataset/uw-enterprises. The original CT data is available as 16-bit tif stacks suitable for analysis with ImageJ (Schneider et al., 2012) or other image analysis software. In addition, videos showing the variation along the length of the cross-section images shown in the previous section are available for download and viewing. A still image from these videos is shown in Figure 28. The red line through the XZ-plane image of the core shows the location of the XY-plane displayed above. The videos on EDX show this XY variation along the entire length of the core.

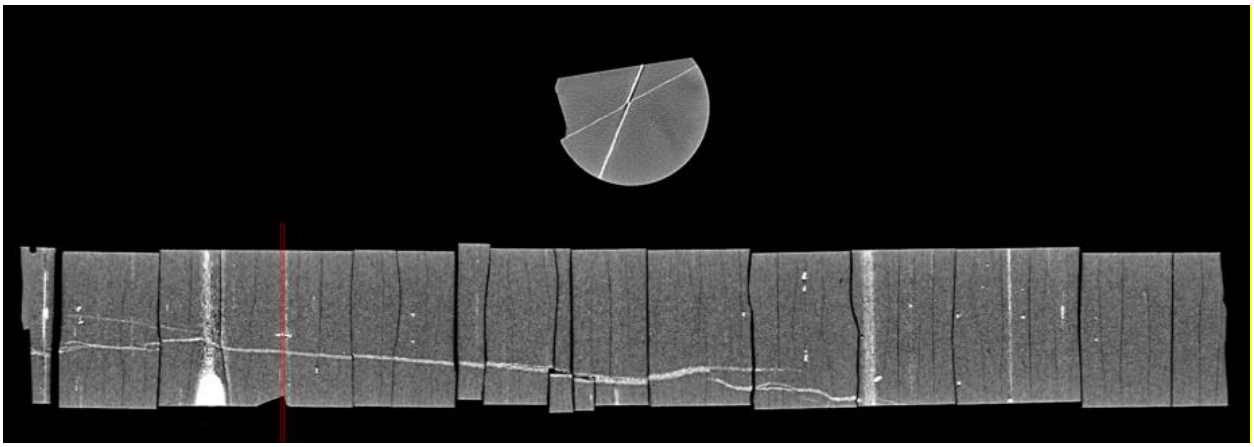

Figure 28: Image still from the medical CT video of the UW Enterprises LP 1-250512-129 well core (4,280 ft to 4,284 ft). Intersecting mineral filled fractures around 4,281 ft can be observed.

4.2.1 Industrial CT Scanning

Detailed scans of sections of interest were performed with Industrial CT. The selected core sections are listed in Table 2 along with the voxel resolution and the image title on EDX. A reslice of each image with a 0.5 mm scale bar is shown in Figure 29 as an example of the industrial CT images.

Table 2: Industrial CT images from UW Enterprises LP 1-250512-129 Well

Depth (ft)	Name	Voxel Resolution (μm^3)
4,219.0	Core 1 Box 10 – 4219.0	55.5
4,257.1	Core 1 Box 10 – 4257.1	58.7
4,256.4	Core 1 Box 23 – 4256.4	58.7
4,199.0	Core 1 Box 4 – 4199.0	57.4
4,202.6	Core 1 Box 5 – 4202.6	57.4

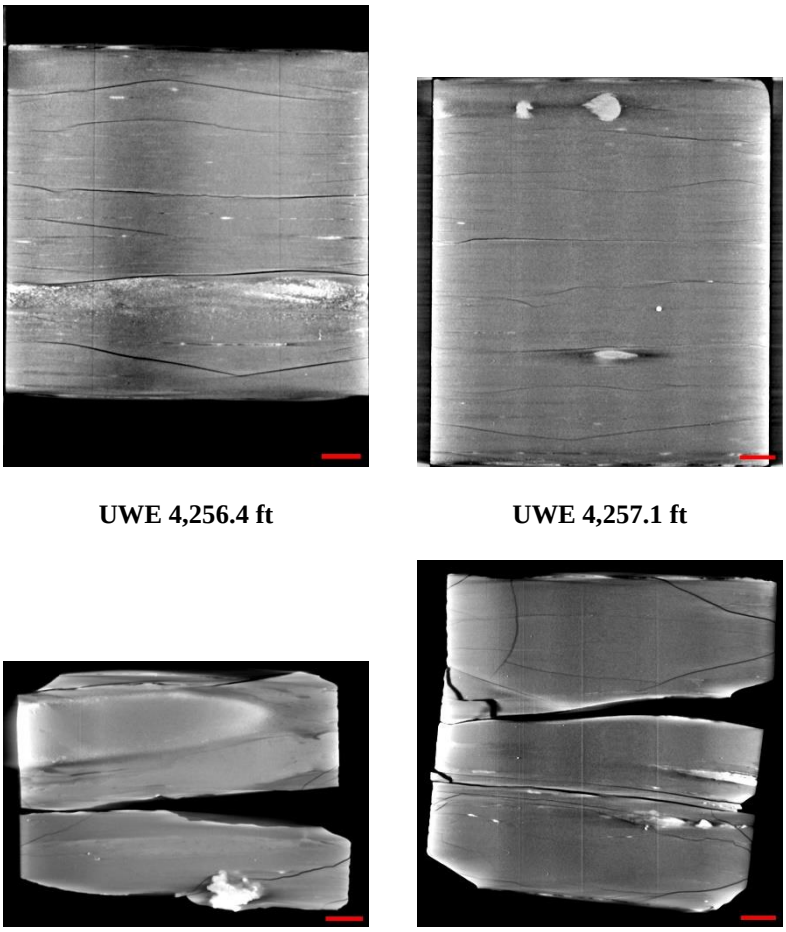

UWE 4,256.4 ft **UWE 4,257.1 ft**

UWE 4,199 ft **UWE 4,202.6 ft**

Figure 29: Reslices from industrial CT images noted in Table 2.

4.2.2 Micro-CT Scanning

A detailed scan of a section of interest was performed using the Xradia CT scanner (Figure 30). A section of core from 4,219 ft was scanned in five sections at a voxel resolution of 1.87 μm^3 and concatenated into a single image. Figure 30 shows an example montage of the micro-CT image volume that is shown in Figure 30, where each image is an isolated slice along the length of the core; note each scale bar represents 0.5 mm.

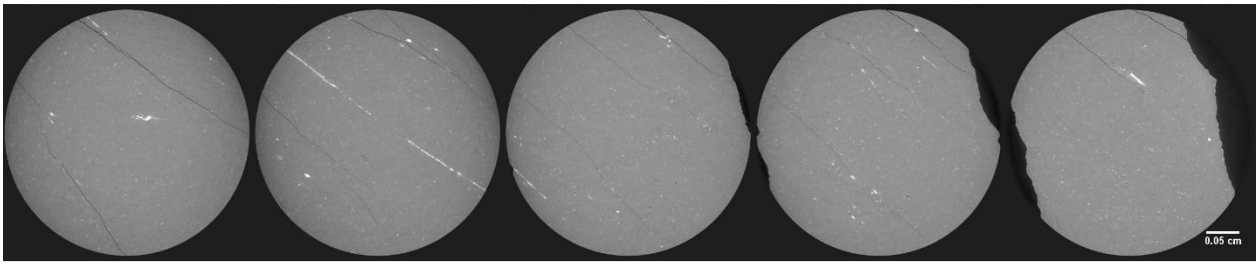

Figure 30: Micro CT image reslices from 4,219 ft.

4.3 DUAL ENERGY CT SCANNING

Dual energy CT scanning uses two sets of images, produced at different X-ray energies, to approximate the density (ρ_B) (Siddiqui and Khamees, 2004; Johnson, 2012). The technique relies on the use of several standards of known ρ_B to be scanned at the same energies as the specimen. These scans are performed at lower energies (<100 KeV) and higher energies (>100 KeV) to induce two types of photon interactions with the object (Figure 31). The lower energy scans induce photoelectric absorption, which occurs when the energy of the photon is completely absorbed by the object mass and causes ejection of an outer orbital electron (Figure 31a). The higher energy scans induce Compton scattering, which causes a secondary emission of a lower energy photon due to incomplete absorption of the photon energy in addition to an electron ejection (Figure 31b).

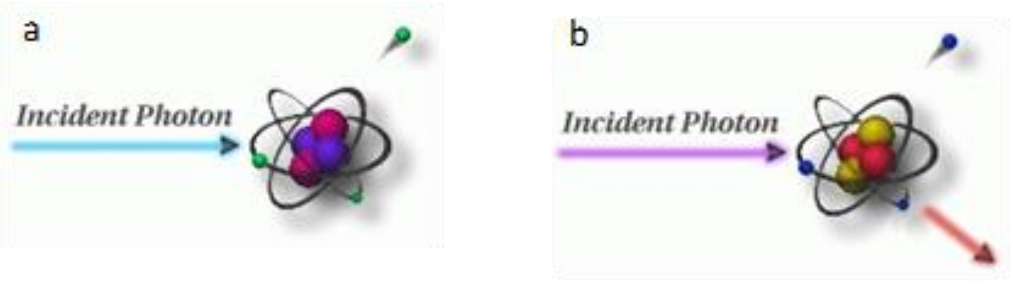

Figure 31: Photon interactions at varying energies. a) Photoelectric absorption, b) Compton scattering. Modified from Iowa State University Center for Nondestructive Evaluation (2021).

Medical grade CT scanners are typically calibrated to known standards, with the output being translated in CTN or Hounsfield Units (HU). Convention for HU defines air as -1,000 and water as 0. A linear transform of recorded HU values is performed to convert them into CTN. This study used CTN as it is the native export format for the instrument, but it is possible to use HU. Dual energy CT requires at least three calibration points, and it is prudent to utilize standards that approximate the object or material of interest. Pure samples of aluminum, graphite, and sodium chloride were used as the calibration standards as they most closely approximate the rocks and minerals of interest (Table 3). Most materials denser than water or with higher atomic masses have a non-linear response to differing CT energies (Table 4).

Table 3: Dual Energy Calibration Standards, Bulk Density (g/cm^3)

Material	ρ_B (g/cm^3)
Air	-0.001
Water	1
Graphite	2.3
Sodium Chloride	2.16
Aluminum	2.7

Table 4: Dual Energy Calibration Standards, HU and CTN for "Low" and "High" Energies

Material	HU		CTN	
	80 KeV	135 KeV	80 KeV	135 KeV
Air	-993	-994	31,775	31,774
Water	-3.56	-2.09	32,764	32,766
Graphite	381	437	33,149	33,205
Sodium Chloride	1,846	1,237	34,614	34,005
Aluminum	2,683	2,025	35,451	34,793

Dual energy CT utilizes these differences to calibrate to the X-ray spectra. Two equations with three unknowns each are utilized to find ρ_B (Siddiqui and Khamees, 2004):

$$\rho_B = mCTN_{low} + pCTN_{high} + q$$

Where [m, p, and q] and [r, s, and t] are unknown coefficients that can be solved by setting up a system of equations with four 3 x 3 determinants. The CTN is obtained from the CT scans for each of the homogenous calibration standards.

In this study, the high and low energy image stacks were loaded into Python as arrays. A 3D Gaussian blur filter with a sigma of 2 was used to reduce noise in the images. The scipy.solv module of Python was then employed to solve for the coefficients based on the calibration CTN values. The ρ_B was solved for each pixel in the 3D volume and saved as two new separate image stacks.

4.4 COMPILED CORE LOG

The compiled core logs were scaled to fit on single pages for rapid review of the combined data from the medical CT and MSCL. Two sets of logs are presented: the first set with data for the major elements and elemental ratios, and the second set with elemental proxies and CT image data. Features that can be derived from these combined analyses include determination of mineral locations, such as pyrite, from magnetic susceptibility. The XRF is used to inform geochemical composition and mineralogy.

Data from the MSCL was filtered to remove areas of fractures and missing core. The P-wave velocity was limited to values greater than 330 m/s as that is the P-wave velocity of air and indicates a lack of solid material at that location. The gamma density and medical CT derived dual energy density, were limited to values greater than 1.5 g/cm^3.

The elemental results from the XRF was used to display U and Th in ppm, and K in %, which providing information on redox state and clay typing, as well as some important elemental proxies related to redox potential (Cr, Co, Ni, Mo, Cu, and V), biogenic production (P, Zn, Y, and V*), skeletal influx/carbonate potential (Ca, Mg, Ba, and Mn), and detrital influence (Zr, Ti, Al, K, and Si).

Trends in elemental ratios can provide insight into variations in mineral composition, oxidation state, and depositional setting. Seven elemental ratios are displayed in tracks 10 and 11. A short description of how these are representative of various geological processes is listed in Table 5.

Table 5: Elemental Ratio and Their Significance

Elemental Ratio	Marker for:	Lower Value	Higher Value
Si/Al	Abundance of illite and micas vs. other clays	More of other clay types	More illite and micas
Ti/Al	Terrigenous input	Less eroded content	More eroded content
Ca/Mg	Dolomite	More dolomitic	Less dolomitic
Ca/Si	Relative abundance of calcium carbonates vs. silicates	Silicate rich	Carbonate rich
S/Fe	Abundance of pyrite (and other iron sulfates) vs. other Fe oxide metals	Fe-oxide dominate/sulfate lean	Sulfate rich
Fe/Al	Degree of pyritization in shales	Lower degree of pyritization	Higher degree of pyritization
Mn/Fe	Oxidation	More anoxic/euxinic	More dysoxic/oxic

The elemental proxy log also includes an XRF “mineralogy” with Al and K, representing clays; Ca, representing calcite; and Si, representing quartz, although there is some Si contribution from the clays. Pyrite (reduced) should have low magnetic susceptibility, and Fe oxide or hydroxide should have high magnetic susceptibility. These broad trends can quickly give information over large lengths of core and direct more focused research to zones of potential interest. These logs are presented in the following image.

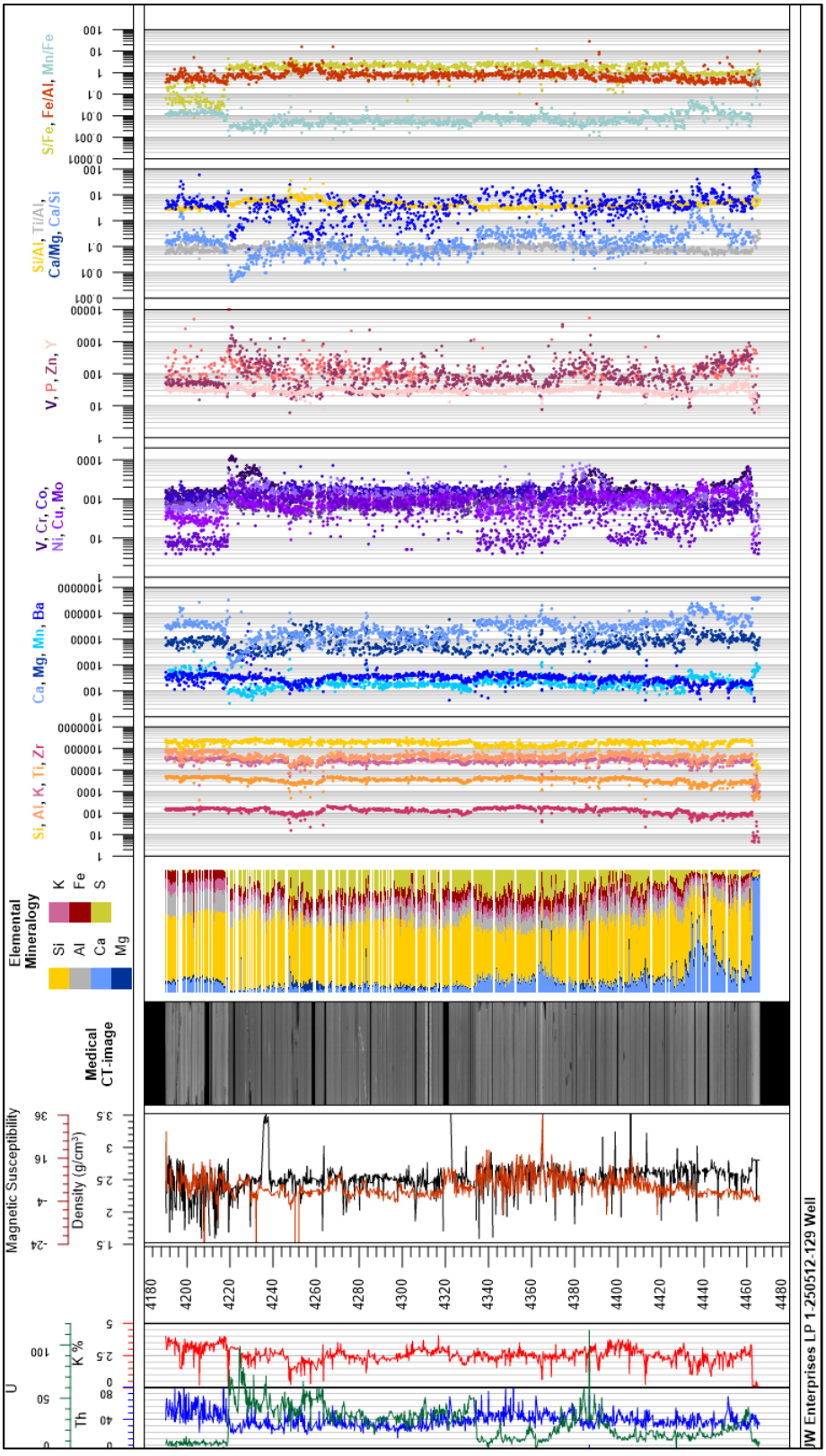

Figure 32: Compiled core log of elemental ratios for the UW Enterprises LP 1-250512-129 Well.

5. DISCUSSION

The measurements of the magnetic susceptibility, gamma density, P-wave velocity, XRF, and CT analysis provide unique insights into of the internal structure of the core and macroscopic changes in lithology. These techniques:

- Are non-destructive.
- When performed in parallel, give insight into the core beyond what one individual technique can provide.
- Can be used to identify zones of interest for more detailed analysis, experimentation, and quantification, for example:
    - Three zones of potential importance for critical mineral exploration can be seen at 4,220 to 4,240 ft, 4,372 to 4,397 ft, and 4,457 to 4,462 ft. These three zones have enrichments of Ni (300 to 500 ppm), V (500 to 1,000 ppm), Cu (~300 ppm), and Zn (200 ppm to 1,200 ppm) coupled with increased values of P and U.
    - Large (1-2 mm) mineral-filled sub-vertical fractures are present from 4,280 to 4,283 ft, and numerous sub-mm fractures are present throughout the New Albany Shale.
    - Bioturbation zones can be seen throughout the New Albany Shale and couple with local increases in Ca and Mg, some burrows appear to be replaced by pyrite (e.g., 4,243 to 4,244 ft).
- Provide a detailed digital record of the core, before any destructive testing or further degradation, that is accessible and can be referenced for future studies.

6. REFERENCES

Finley, R. J. An overview of the Illinois Basin–Decatur project. Greenhouse Gases: Science and Technology **2014,** *4*, 571–579.

Geotek Ltd. Multi-Sensor Core Logger Manual; Version 05-10; Published by Geotek, 3 Faraday Close, Daventry, Northamptonshire NN11 8RD, 2010. www.geotek.co.uk

Hunts, C.; Moskowitz, B.; Banerjee, S. *Magnetic Properties of Rocks and Minerals;* Rock Physics and Phase Relations: A Handbook of Physical Constants; 1995; p 189-204.

Iowa State University Center for Nondestructive Evaluation, Ames, IA, 2021. https://www.nde-ed.org/Physics/X-Ray/attenuation.xhtml (accessed July 2021).

Johnson, T. R. C. Dual-Energy CT: General Principles. *American Journal of Roentgenology* **2012,** *199*, S3–S8. DOI: 10.2214/AJR.12.9116.

Schneider, C. A.; Rasband, W. S.; Eliceiri, K. W. NIH Image to ImageJ: 25 years of image analysis. *Nature Methods* **2012,** *9*, 671–675.

Siddiqui, S.; Khamees, A. A. Dual-Energy CT-Scanning Applications in Rock Characterization. *Society of Petroleum Engineers* **2004**. DOI:10.2118/90520-MS.

Strąpoć, D.; Mastalerz, M.; Schimmelmann, A.; Drobniak, A.; Hasenmueller, N. R. Geochemical constraints on the origin and volume of gas in the New Albany Shale (Devonian–Mississippian), eastern Illinois Basin. *AAPG Bulletin* **2010,** *94*, 1713–1740.

This page intentionally left blank.

Marianne Walck
Director
National Energy Technology Laboratory
U.S. Department of Energy

Jessica Mullen
Critical Minerals and Materials
Technology Manager
National Energy Technology Laboratory
U.S. Department of Energy

Mary Anne Alvin
Critical Minerals and Materials Program
Manager
Office of Resource Sustainability
U.S. Department of Energy

Bryan Morreale
Executive Director
Research and Innovation Center
National Energy Technology Laboratory
U.S. Department of Energy